Inverse Modeling of Facial Contact

Moritz Bächer

Master Thesis
November 18, 2008

Advisor: Bernd Bickel
Supervisor: Prof. Dr. Markus Gross

ETH
Eidgenössische Technische Hochschule Zürich
Swiss Federal Institute of Technology Zurich

cgl
Computer Graphics Laboratory ETH Zurich

Abstract

In this thesis, a novel representation and technique for simulating static non-linear material behavior based on Finite Elements (FE) is presented. All required simulation parameters can be acquired and fitted from a set of example deformations of a real-word object or subject. The simulation is therefore closely related to the person or object specific deformation behavior. We first acquire a single static surface scan and several measurements of static surface displacements by probing an object at many positions and orientations using a force sensor. A trinocular stereo system measures the surface displacements at colored marker locations on the object. The volume of the object is discretized into tetrahedral elements, and for each element and every measurement material parameters are fitted. Our material model consists of material parameters and the corresponding material strain. During run time, we blend these parameters by using a novel strain-based interpolation scheme in material strain space, modeling therefore intuitively the non-linear material stress-strain relationship. Furthermore, since the model is based on a linear deformation FEM simulations of new interactions are stable and also computationally efficient.

Acknowledgment

I would like to thank all people who have helped and inspired me during my master thesis.

I especially want to thank my advisor, Bernd Bickel, for all the fruitful discussions and all the patience he had with me. I also wish to express my warm thanks to my supervisors, Professor Markus Gross (ETH Zurich), and Professor Hanspeter Pfister (Harvard University), for their valuable advice and friendly help. Professor Miguel A. Otaduy (URJC Madrid) and Doctor Wojciech Matusik (Adobe Research) also deserve a special thanks as collaborators on this work.

My deepest gratitude goes to my extended family and friends.

Lastly, and most importantly, I wish to thank my parents, Esther and Martin Bächer for all their love and support.

Contents

List of Figures

List of Tables

1

Introduction

Creating visually accurate models of real-world objects is a fundamental problem in computer graphics. Since most objects in our physical world are not rigid, it is not sufficient to simply capture their static geometry and appearance. We also need to measure how an object deforms upon contact and incorporate this *contact interaction behavior* in its model.

Finding a general model of deformable objects that allows physically-plausible simulation in space and time is very challenging. Potential applications require such a model to cover conflicting demands: For a special effect animator, for example, a physically-accurate interaction behavior is essential when animating a natural phenomena. On the other hand, feedback has to be fast enough to be useful in his work flow. In virtual realities, this interactivity requirement is even more crucial while realistic rendering is still of high importance.

Most deformable models in computer graphics are solving a so-called *direct problem*. That is, the deformation response of an object given a specific contact is determined by assuming that a set of model parameters is known. The model parameters often have to be adjusted by hand and the resulting simulated deformation behavior approximates real-world behavior rather poorly. The fundamental observation on which our approach is based on is that accurate *direct analysis* can only be made when *inverse analysis* has been solved to determine the *requisites*, such as model parameters, for the direct problem.

To increase realism in simulations of deformable objects, models based on *continuum mechanics* have been extensively used in the graphics community. The field of continuum mechanics provides a comprehensive theoretical framework for the analysis of the *mechanical behavior* of materials and therefore leads to more accurate deformable models. Within this theory, deformable objects are modeled as so-called *solid continua*. That is, the matter of an object is assumed to be *continuously distributed* over the region of the space it occupies. This assumption allows to describe the mechanical behavior of an object by a set of Partial Differential Equations

(PDE's). These PDE's are of two main kinds: Firstly, there are equations such as conservation laws which apply equally to all materials. Secondly, there are equations - known as *constitutive equations* - which describe the mechanical behavior of particular materials. By discretizing the involved equations using, for instance, Finite Elements (FE's) a specific mechanical behavior can be simulated on a computer.

The PDE's of a general deformable object are *non-linear* and a discretization of the governing equations using the Finite Element Method (FEM) yields a set of non-linear algebraic equations. Solving such a *non-linear system of equation* is computationally very costly and can also be numerically unstable. The governing PDE's are therefore often *linearized*. This linearization leads to a *linear system of equations* whose solution is fast to compute and also numerically stable. However, it also entails significant linearization artifacts during a simulation.

Our approach fills the gap between a computationally efficient linear and a physically-accurate non-linear FEM approach by incorporating measured deformation behavior into a FEM-based deformation model. We first refine a linear FEM model while keeping it computationally efficient. To this end, we increase the number of model or more precisely material parameters and also integrate a *warped stiffness* approach [Müller et al. 2002, Müller and Gross 2004]. By substituting measured *contact interactions* into the governing finite equations and by *inversely* using them we are able to formulate an *inverse problem* from which the unknown *material parameters* can be obtained. During simulations of new contact interactions the fitted FEM-approximations are *blended* together by interpolating between estimated parameters in parameter space.

The thesis is organized as follows. In Chapter 2 connections to related work are discussed. We then start with a direct analysis of a general contact interaction (Chapter 3). In Chapter 4 we discuss the acquisition of contact measurements which are then used in the subsequent Chapter 5 to formulate our inverse problem. The simulation of new interactions is discussed in Chapter 6. It follows a Chapter in which the model is validated (Chapter 7). In Chapter 8 conclusions are drawn and future work is discussed.

2

Related Work

Since Terzopoulos et al.'s paper about elastically deformable models [Terzopoulos et al. 1987], physically-based deformation models have been an active research area in computer graphics. A wide range of models were proposed and the interested reader is referred to two survey papers [Gibson and Mirtich 1997, Nealen et al. 2005]. In this thesis the discussion of related work focuses on mesh-based methods only:

Mass-Spring Systems. Among mesh based methods, the most simple, and hence most popular deformable model is a mass-spring system. The model is discrete in nature and not derived from a set of partial differential equations. The technique allows to model static and dynamic deformations and has even been extended to model non-linear behavior [Yu et al. 2001]. However, its parameterization based on spring constants is not directly related to the constitutive equations of a specific object. Fitting and validation of parameters is therefore difficult [Bianchi et al. 2004]. Furthermore, a large number of nodes is needed to compensate for the model's inaccuracies which in turn increases the model's computational cost.

Models Based on Finite Differences. The Finite Difference Method (FDM) provides an easy way of discretizing PDE's and was, for instance, used by Terzopoulos et al. to discretize their deformation model [Terzopoulos et al. 1987]. The assumption of a regular mesh, however, makes it difficult to approximate an object's boundary.

Models Based on Boundary Elements. A deformation model based on boundary integrals and the Boundary Element Method (BEM) was first used in graphics by [James and Pai 1999]. Given that our measurements are only capturing the interaction behavior on an object's boundary, a BEM formulation would simplify our parameter fitting notably. But the class of materials the method can handle is restricted to those with *homogeneous* properties. Extending such a model to include more complex behavior is not straight-forward.

Models Based on Finite Elements. The finite element method, even though more complex, provides more flexibility. It was successfully and extensively used by material scientists to model linear and non-linear continua. Excellent introductions to linear and non-linear FEM-based deformation models are given in [Bathe 1995, Bonet and Wood 2008].

Our approach is based on the warped stiffness approach described in [Müller and Gross 2004]. Stiffness warping helps to remove the artifacts that linear FEM models show if large rotational deformations are applied. Linear FEM models assume a linearized Green strain which is not rotation-invariant. This assumption may lead to ghost forces during a simulation, which in turn can cause unrealistic growth in volume. The ghost forces can be avoided by computing the element forces in unrotated frames before rotating them back to the frames of the deformed elements. In contrast to [Müller and Gross 2004], we employ stiffness warping in a *static* FEM model.

Inverse Problems and the Theory of Regularization. The determination of material parameters from observed deformation responses involves solving an inverse problem. Inverse problems, in contrast to direct problems, are often *ill-posed*. The *theory of regularization* provides powerful techniques to solve such problems by adding *smoothness constraints*. An overview over those techniques for linear and non-linear inverse problems is given in [Hansen 2007] and [Engl and Kügler 2003], respectively.

Blending Techniques. We use a technique similar to the weighted pose-space deformation (WPSD) scheme of [Bickel et al. 2008] to interpolate between the estimated material parameters in parameter space. This RBF-based interpolation technique (RBF stands for Radial Basis Function [Carr et al. 2001]) allows us to *blend* between fitted FEM approximations during simulations of new contact interactions. As arguments to the RBF's, a novel weighted *strain-based* distance metric is used.

Scanning Physical Interaction Behavior. Most related to the work presented here is the work by Pai et al. [Pai et al. 2001] about scanning the physical interaction behavior of objects. They built a highly automated robotic measurement facility to measure the physical interaction behavior of objects. In contrast to our work, their model is only able to capture the linear behavior of an object.

3

Direct Analysis of Contact Interaction

In this chapter we analyze an individual *contact interaction* with a *solid object* as a *direct problem*. For a direct problem to be posed, several *requisites* have to be met. In our case the knowledge of the following items are required:

- *Region of space* the deformable object occupies.
- *Governing equations* that describe the deformation behavior in the interior of the object.
- Prescribed displacements and applied forces which act as *constraints* on the object's surface.
- The object's *material properties*.

When all of these requisites are satisfied, the *deformation response* of a specific contact interaction can be computed by using a discretization scheme, such as the finite element method.

We start with a *linear analysis* of the mechanics of a general contact interaction and assume the object's material properties to be *homogenous* and *isotropic*. That is, the material properties are assumed to be the same throughout the object's body and also independent of direction. However, the assumption of translational and rotational invariant material properties does not hold for general deformable objects. We therefore refine the parameterization of the linear formulation so that *inhomogeneous* and *pseudo-anisotropic* material behavior can be efficiently approximated.

This refinement of material parameters does not avoid all of the linearization artifacts. The linearization of material-independent or so-called *non-constitutive* equations may also lead to significant artifacts especially in case of large rotational deformations. We therefore employ warped stiffnesses [Müller et al. 2002, Müller and Gross 2004] in our model which provide a robust and effective way to avoid those non-constitutive artifacts.

3.1 Linear Analysis of Solid Continua

Before we start with the linear analysis of a deformable object we first restate our direct problem on a more abstract level. Thereafter, the two major physical quantities, namely the *strain* and *stress tensors*, are introduced. Those quantities are then used to derive the *governing equations* within the object's body. The governing equations, in turn, allow us to describe the unknown deformation response as a minimum of an *equilibrium equation*. By using a *finite element discretization* of the involved physical quantities the deformation response can be found by solving a simple linear *system of finite equations*.

3.1.1 Problem Statement

A general deformable object in its rest and deformed state is illustrated in Figure 3.1.

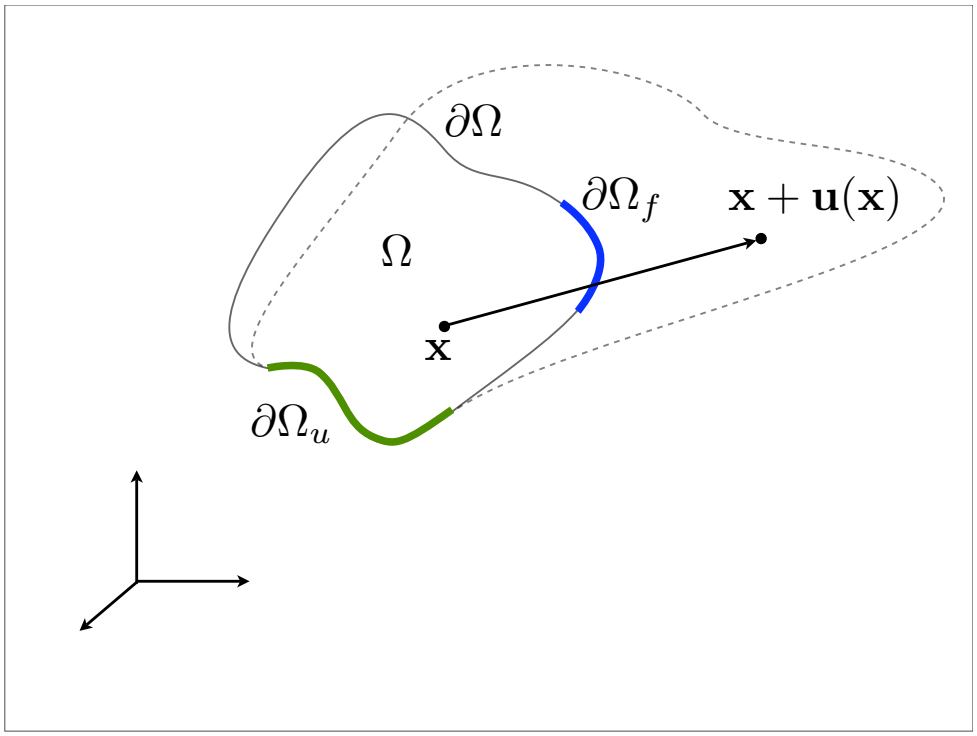

Figure 3.1: *A general deformable object in its rest and deformed state. Geometric constraints are painted green and force constraints are painted blue.*

As mentioned above, the deformation response of a deformable object on a specific contact can only be computed if a set of requisites is known. We repeat those requisites and state our problem in more mathematical terms here:

The following four requisites have to be met so that direct analysis can be applied to calculate the response of a deformable object upon a contact:

- The *domain* Ω and *boundary* $\partial\Omega$ of the deformable object in its rest state.
- The *governing PDE's* in the domain Ω.

- The two kinds of *boundary conditions*: Geometric constraints and force constraints.
- The *material parameters* involved in the governing PDE's.

We have two kinds of boundary conditions in our problem. On one hand, we assume that parts of the object's boundary is fixed. We denote those parts as $\partial\Omega_u$ and call those kinds of conditions *geometric constraints*. More interestingly are the parts of the surface where we apply our contact forces. These parts are denoted as $\partial\Omega_f$ and the corresponding conditions are called *force constraints*.

We observe that a specific deformation response can be described as a displacement field

$$\mathbf{u}(x,y,z) = \begin{bmatrix} u(x,y,z) \\ v(x,y,z) \\ w(x,y,z) \end{bmatrix} \tag{3.1}$$

that relates every point $\mathbf{x} \in \Omega$ of the body in its rest state to the corresponding point $\mathbf{x} + \mathbf{u}(\mathbf{x})$ in its deformed state.

Our goal is therefore to find this displacement field $\mathbf{u}(\mathbf{x})$.

3.1.2 Strain-Displacement Relation

In the next two Subsections, we introduce the two major physical quantities that describe the deformation behavior in the interior of an object. The resulting two equations, namely the *strain-displacement* and the *strain-stress relation*, describe the *non-constitutive* and *constitutive* behavior of a specific object. We start our discussion by introducing the so-called strain tensor:

Strain tensors provide a powerful mathematical tool to describe local deformations in the interior of an object. Two typical choices are given by the non-linear Green strain and its linearized version, the Cauchy strain. We employ the linear Cauchy strain in our work which is defined as:

$$\varepsilon(\mathbf{u}) = \frac{1}{2}\left(\nabla\mathbf{u} + (\nabla\mathbf{u})^T\right) \tag{3.2}$$

By using a linearized version of the Green strain we loose its rotational-invariance property. This, in turn, leads to significant linearization artifacts in case of large rotational deformations. However, as mentioned before, those artifacts can effectively be eliminated by using a warped stiffness approach [Müller and Gross 2004]. We will get back to that in Section 3.3.

The Cauchy strain is symmetric. This symmetry property can be used to rewrite the 3×3 tensor

as a 6×1 vector:

$$\varepsilon(\mathbf{u}) = \begin{pmatrix} u_x & u_y + v_x & u_z + w_x \\ v_x + u_y & v_y & v_z + w_y \\ w_x + u_z & w_y + v_z & w_z \end{pmatrix} \quad \longrightarrow \quad \varepsilon(\mathbf{u}) = \begin{bmatrix} u_x \\ v_y \\ w_z \\ v_x + u_y \\ w_y + v_z \\ w_x + u_z \end{bmatrix} \tag{3.3}$$

By introducing a linear differential operator D, we can finally write the Cauchy strain as a linear strain-displacement relation:

$$\varepsilon(\mathbf{u}) = D\mathbf{u} \tag{3.4}$$

with

$$D = \begin{bmatrix} \frac{\partial}{\partial x} & 0 & 0 \\ 0 & \frac{\partial}{\partial y} & 0 \\ 0 & 0 & \frac{\partial}{\partial z} \\ \frac{\partial}{\partial y} & \frac{\partial}{\partial x} & 0 \\ 0 & \frac{\partial}{\partial z} & \frac{\partial}{\partial y} \\ \frac{\partial}{\partial z} & 0 & \frac{\partial}{\partial x} \end{bmatrix} \tag{3.5}$$

3.1.3 Stress-Strain Relation

Strain leads to internal forces which are represented by a so-called stress tensor σ. We observe that the symmetry property also holds for the 3×3 stress tensor. The stress-strain relation can therefore be written as

$$\sigma(\mathbf{u}) = \mathbf{E}\varepsilon(\mathbf{u}) \tag{3.6}$$

if a homogenous linear material is assumed. This relation is also known as *Hooke's law of elasticity*. The 6×6 matrix $\mathbf{E}$ is material dependent and allows us to simulated different material behavior by changing its entries. The above relation belongs therefore to the class of constitutive equations.

The assumption of a linear strain-stress relation is only valid for linear materials or, in case of non-linear materials, only if sufficiently small deformations are applied. A major contribution of our work is that non-linear stress-strain relations can be approximated by fitting and blending individual linear FEM-approximations.

3.1.4 Equilibrium Equation

The solution to our problem is the displacement field that describes the deformed object in its *condition of equilibrium*. We therefore recast our constrained problem in terms of an *equilib-*

rium equation. To this end, we first have to define the *internal* and *external energies* inherent in the problem:

The total internal energy of a deformable object is defined as:

$$I(\mathbf{u}) = \frac{1}{2}\int_{\Omega} \varepsilon(\mathbf{u})^T \sigma(\mathbf{u}) d\mathbf{x} \tag{3.7}$$

In our case, the only source of external energy is given by the constraints on the object's boundary. For simplicity, we only discuss the effect of force constraints here and postpone the discussion of geometric constraints to Subsection 3.1.7.

The external energy, or more precisely the *external work*, that is added to the body through the force constraints in the contact areas $\partial\Omega_f$ is given by:

$$W(\mathbf{u}) = \int_{\partial\Omega_f} \mathbf{f}^T \mathbf{u} d\mathbf{x} \tag{3.8}$$

where $\mathbf{f}(\mathbf{x})$ is the force field defined at every point $\mathbf{x} \in \partial\Omega_f$.

The equilibrium equation of our problem is thus

$$E(\mathbf{u}) = I(\mathbf{u}) - W(\mathbf{u}) = \frac{1}{2}\int_{\Omega} \varepsilon(\mathbf{u})^T \sigma(\mathbf{u}) d\mathbf{x} - \int_{\partial\Omega_f} \mathbf{f}^T \mathbf{u} d\mathbf{x} \tag{3.9}$$

and the displacement field $\mathbf{u}$ that minimizes $E(\mathbf{u})$ is the deformation we are looking for.

3.1.5 Finite Element Approximation of Fields

So far, we described the continuum behavior of an object at an infinity of points. The next step is to discretize this behavior in terms of a finite number of points called *nodes*. To this end, the object is partitioned into a set of *finite elements* e. The partition we use in our work is based on *tetrahedral elements*.

This discretization of space allows us to approximate the displacement field $\mathbf{u}(\mathbf{x})$ within a specific element e by interpolating the nodal displacements $\mathbf{u}_i^e$ (displacement at node $\mathbf{x}_i^e$) by using a set of *basis functions* $\phi_i^e(\mathbf{x})$:

$$\mathbf{u}(\mathbf{x})|_e \approx \sum_{i=1}^{4} \mathbf{u}_i^e \phi_i^e(\mathbf{x}) \tag{3.10}$$

We employ *linear* basis functions in our finite element approximation. The coefficients of the basis function

$$\phi_i^e(x, y, z) = a_i^e x + b_i^e y + c_i^e z + d_i^e \tag{3.11}$$

corresponding to node i of element e can be found by solving the equation system:

$$\phi_i^e(\mathbf{x}_j^e) = \delta_{ij}, j = 1, \ldots, 4 \tag{3.12}$$

where δ_{ij} denotes the Kronecker delta.

By introducing a 3×12 matrix

$$\mathbf{H}_e(\mathbf{x}) = [\mathbf{H}_1^e(\mathbf{x})\, \mathbf{H}_2^e(\mathbf{x})\, \mathbf{H}_3^e(\mathbf{x})\, \mathbf{H}_4^e(\mathbf{x})] \tag{3.13}$$

with elements

$$\mathbf{H}_i^e(\mathbf{x}) = \mathrm{diag}(\phi_i^e(\mathbf{x}),\, \phi_i^e(\mathbf{x}),\, \phi_i^e(\mathbf{x})) \tag{3.14}$$

and collecting all nodal displacements $\mathbf{u}_i^e$ in a 12×1 vector $\mathbf{u}_e$, the approximated displacement field within an element e can be written as a matrix-vector multiplication:

$$\mathbf{u}(\mathbf{x})|_e \approx \mathbf{H}_e(\mathbf{x})\mathbf{u}_e \tag{3.15}$$

The discretized displacement field, in turn, allows us to derive discrete versions of element strains and element stresses:

The discretized strain within an element e is

$$\varepsilon(\mathbf{x})|_e \approx \varepsilon_e(\mathbf{x}) = D\mathbf{H}_e(\mathbf{x})\mathbf{u}_e \tag{3.16}$$

If we now apply the differential operator D to the matrix $\mathbf{H}_e$, we get a constant 6×12 matrix $\mathbf{B}_e$. The discrete strain is therefore assumed to be constant within an element and is given by:

$$\varepsilon(\mathbf{x})|_e \approx \mathbf{B}_e\mathbf{u}_e \tag{3.17}$$

The discrete stress tensor within an element e is simply

$$\sigma(\mathbf{x})|_e \approx \mathbf{E}\varepsilon_e \tag{3.18}$$

if a homogenous and linear material is assumed.

Both, the discretized stress and strain tensor fields are thus assumed to be element-wise constant.

3.1.6 Discrete Equilibrium Equation

With the discrete versions of the displacement and the two tensor fields we can finally derive a discrete version of our equilibrium equation.

Let us first start with the discretization of the internal energy. As we saw in Subsection 3.1.4 Equation 3.7, the total internal energy of a deformable body is defined as:

$$I(\mathbf{u}) = \frac{1}{2}\int_\Omega \varepsilon(\mathbf{u})^T\sigma(\mathbf{u})d\mathbf{x}. \tag{3.19}$$

A discretized version of the internal energy can be derived by simply replacing the global strain and stress tensor fields by their element-wise constant approximations:

$$I(\mathbf{u}) \approx \frac{1}{2}\sum_e \int_{V_e} \varepsilon_e^T\mathbf{E}\varepsilon_e = \frac{1}{2}\sum_e \mathbf{u}_e^T\left(\int_{V_e}\mathbf{B}_e^T\mathbf{E}\mathbf{B}_e\right)\mathbf{u}_e \tag{3.20}$$

The integral in brackets is the so-called stiffness matrix of element e, denoted as $\mathbf{K}_e$. Because of the constancy of both, the element strains and element stresss, the integral over the element's volume V_e simplifies to a multiplication by V_e:

$$\mathbf{K}_e = \int_{V_e} \mathbf{B}_e^T \mathbf{E} \mathbf{B}_e = V_e \mathbf{B}_e^T \mathbf{E} \mathbf{B}_e \tag{3.21}$$

The discrete internal energy can therefore be written as a closed form:

$$I(\mathbf{u}) \approx \frac{1}{2} \sum_e \mathbf{u}_e^T \mathbf{K}_e \mathbf{u}_e = \frac{1}{2} \mathbf{u}^T \mathbf{K} \mathbf{u} \tag{3.22}$$

The matrix $\mathbf{K}$ is the so-called global stiffness matrix and has $3n \times 3n$ elements if n denotes the number of nodes. Its assembly from element stiffnesses will be discussed in Subsection 3.1.8. All the nodal displacements are collected in the $3n \times 1$ vector $\mathbf{u}$. Note that we used the same notation for the displacement field and its discrete counterpart here. In the following, $\mathbf{u}$ is exclusively used for discrete displacement field if not mentioned otherwise.

Next, we will discretize the external energy. According to Equation 3.8, the external work is defined as:

$$W(\mathbf{u}) = \int_{\partial\Omega_f} \mathbf{f}^T \mathbf{u} d\mathbf{x} \tag{3.23}$$

The discretized force field is only defined for nodes part of the surface area $\partial\Omega_f$. To simplify our notation, we assume that forces are defined at all nodes of the discretization and that they are only non-zero if the corresponding node is part of $\partial\Omega_f$. This allows us to write the discretized external energy as:

$$W(\mathbf{u}) \approx \sum_{j=1}^{n} \mathbf{f}_j^T \mathbf{u}_j = \mathbf{f}^T \mathbf{u} \tag{3.24}$$

where the sum is over all nodes and the $\mathbf{f}$ and $\mathbf{u}$ denote the two $3n \times 1$ vectors which collect the nodal forces and displacements.

The discrete equilibrium equation can therefore be written as a quadratic form:

$$E(\mathbf{u}) \approx \frac{1}{2} \mathbf{u}^T \mathbf{K} \mathbf{u} - \mathbf{f}^T \mathbf{u} \tag{3.25}$$

The displacement vector that minimizes this discretized energy equation can be found by setting the gradient with respect to $\mathbf{u}$ of the above expression to zero (note that the global stiffness matrix is symmetric):

$$\nabla_{\mathbf{u}} \left[\frac{1}{2} \mathbf{u}^T \mathbf{K} \mathbf{u} - \mathbf{f}^T \mathbf{u} \right] = \mathbf{K} \mathbf{u} - \mathbf{f} = \mathbf{o} \tag{3.26}$$

The displacement can therefore be found by solving a linear system of finite equations:

$$\mathbf{K} \mathbf{u} = \mathbf{f} \tag{3.27}$$

3.1.7 Geometric Constraints

In the above derivation, we only discussed the effect of force constraints. Let us now take a closer look at the effect of geometric constraints.

Without loss of generality (renumbering of nodes), the equation system

$$\mathbf{K}\mathbf{u} = \mathbf{f} \tag{3.28}$$

can be reformulated as:

$$\begin{bmatrix} \mathbf{K}_{\partial\Omega_f,\partial\Omega_f} & \mathbf{K}_{\partial\Omega_f,\Omega} & \mathbf{K}_{\partial\Omega_f,\partial\Omega_u} \\ \mathbf{K}_{\Omega,\partial\Omega_f} & \mathbf{K}_{\Omega,\Omega} & \mathbf{K}_{\partial\Omega,\partial\Omega_u} \\ \mathbf{K}_{\partial\Omega_u,\partial\Omega_f} & \mathbf{K}_{\partial\Omega_u,\Omega} & \mathbf{K}_{\partial\Omega_u,\partial\Omega_u} \end{bmatrix} \begin{bmatrix} \mathbf{u}_{\partial\Omega_f} \\ \mathbf{u}_{\Omega} \\ \mathbf{u}_{\partial\Omega_u} \end{bmatrix} = \begin{bmatrix} \mathbf{f}_{\partial\Omega_f} \\ \mathbf{f}_{\Omega} \\ \mathbf{f}_{\partial\Omega_u} \end{bmatrix} \tag{3.29}$$

The subscripts are self-explanatory. $\mathbf{u}_{\partial\Omega_f}$, for instance, is the vector which collects all the displacements of nodes that are part of $\partial\Omega_f$. For simplicity, we use Ω instead of $\Omega\backslash(\partial\Omega_u \cup \partial\Omega_f)$ to describe the set of all nodes except those part of $\partial\Omega_u$ or $\partial\Omega_f$. According to our problem statement (geometric constraints), the nodes on the discretized surface area $\partial\Omega_u$ are assumed to be fixed. In other words, $\mathbf{u}_{\partial\Omega_u}$ is assumed to be equal to the zero vector. Furthermore, we assumed that nodal forces are only non-zero for nodes part of $\partial\Omega_f$. Hence, $\mathbf{f}_{\partial\Omega_u}$ and $\mathbf{f}_{\partial\Omega}$ are equal to the zero vector as well.

The system therefore reduces to:

$$\begin{bmatrix} \mathbf{K}_{\partial\Omega_f,\partial\Omega_f} & \mathbf{K}_{\partial\Omega_f,\Omega} \\ \mathbf{K}_{\Omega,\partial\Omega_f} & \mathbf{K}_{\Omega,\Omega} \end{bmatrix} \begin{bmatrix} \mathbf{u}_{\partial\Omega_f} \\ \mathbf{u}_{\Omega} \end{bmatrix} = \begin{bmatrix} \mathbf{f}_{\partial\Omega_f} \\ \mathbf{o} \end{bmatrix} \tag{3.30}$$

3.1.8 Matrix Assembly

The global stiffness matrix $\mathbf{K}$, as defined in Equation 3.22, has to be assembled from the individual element stiffnesses $\mathbf{K}_e$. To this end, the 12×12 stiffnesses $\mathbf{K}_e$ are first split into 16 block matrices. Those 3×3 blocks are then added to the corresponding blocks in the global matrix $\mathbf{K}$ as illustrated in Figure 3.2.

For simplicity of notation, a sigma sign is used to abbreviate this special assembly procedure:

$$\mathbf{K} = \sum_e \mathbf{K}_e \tag{3.31}$$

In the following summations over elements ($\sum_e$) indicate that a global matrix has to be assembled from12×12 element matrices.

3.2 Material Properties

In the last Section, we assumed a globally constant material matrix $\mathbf{E}$. That is, we assumed the material properties to be homogenous throughout the object's body. $\mathbf{E}$ itself has still 36 degrees

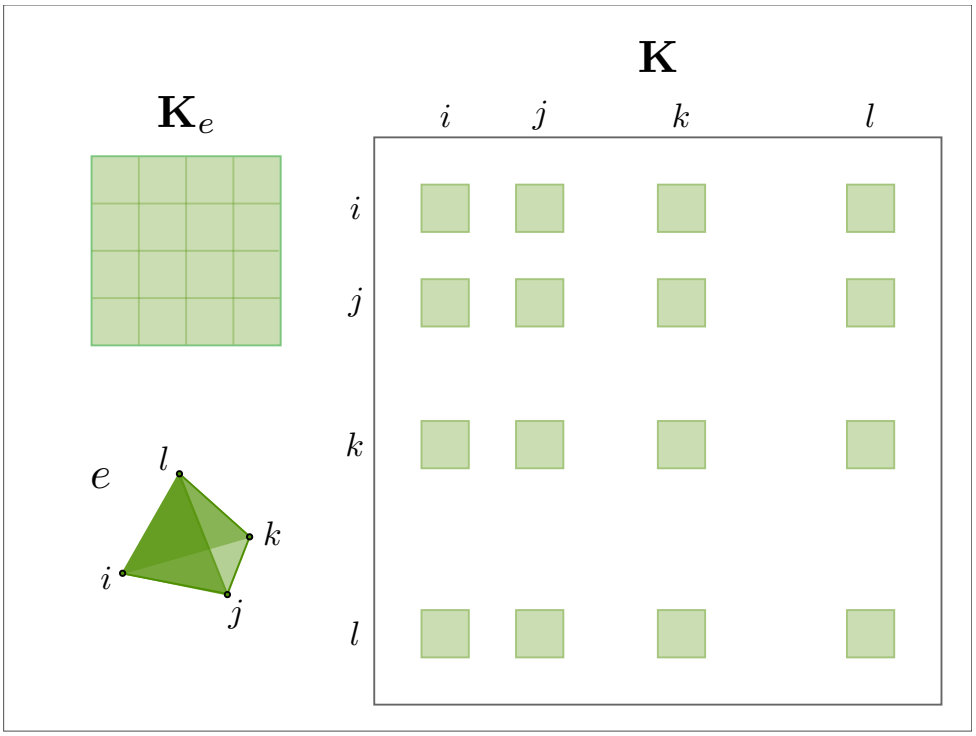

Figure 3.2: *Matrix assembly: i, j, k, l denote the global indices of the nodes of element e.*

of freedom which allow us to have properties that vary across global directions. In this Section, we will introduce homogenous materials that exhibit the same material properties across all global directions, so-called isotropic materials. This isotropy assumption allows to reduce the number of global variables to a set of two independent elastic constants. These two constants are usually expressed as Young's modulus E and Poisson ratio ν and our material matrix $\mathbf{E}$ can be written as:

$$\mathbf{E} = \frac{E}{(1+\nu)(1-2\nu)} \left(\mathbf{F} + \nu \mathbf{G}\right) \tag{3.32}$$

with the two constant matrices

$$\mathbf{F} = \begin{bmatrix} 1 & 0 & 0 & 0 & 0 & 0 \\ 0 & 1 & 0 & 0 & 0 & 0 \\ 0 & 0 & 1 & 0 & 0 & 0 \\ 0 & 0 & 0 & 0.5 & 0 & 0 \\ 0 & 0 & 0 & 0 & 0.5 & 0 \\ 0 & 0 & 0 & 0 & 0 & 0.5 \end{bmatrix} \tag{3.33}$$

and

$$\mathbf{G} = \begin{bmatrix} -1 & 1 & 1 & 0 & 0 & 0 \\ 1 & -1 & 1 & 0 & 0 & 0 \\ 1 & 1 & -1 & 0 & 0 & 0 \\ 0 & 0 & 0 & -1 & 0 & 0 \\ 0 & 0 & 0 & 0 & -1 & 0 \\ 0 & 0 & 0 & 0 & 0 & -1 \end{bmatrix} \tag{3.34}$$

Let us briefly discuss the meanings of these two elastic constants:

Poisson ratio The Poisson ratio is unit-less and describes the compressibility of a material. The range of physically-plausible values is $-1 < \nu < 0.5$. Negative Poisson ratios are rare. Materials with a negative Poisson ratio become thicker in one direction if they are stretched in perpendicular directions. Hence, most materials have a Poisson ratio between 0.0 and 0.5. A Poisson ratio of nearly 0.5 means the material is almost incompressible.

Young's Modulus The Young's modulus of a material is usually given in Giga Pascal ($GPa = 10^9 \frac{N}{m^2}$ and is always positive. To ease the discussion of fitted parameters in Chapter 7, the conversion factor between table values (in GPa) and our parameter values (which are given in $\frac{N}{cm^2}$ because displacements are measured in cm) is calculated here:

$$1GPa = 10^9 \frac{N}{m^2} = 10^9 \frac{N}{(100cm)^2} = 10^5 \frac{N}{cm^2} \tag{3.35}$$

We therefore have to multiply table values by a factor of 10^5 to compare them with our fitted Young's moduli.

A parameterization of homogeneous isotropic materials based on the Poisson ratio and the Young's modulus is more intuitive then others. However, we employ an alternative parameterization in our work which allows us to write the matrix $\mathbf{E}$ as a linear combination of the two constant matrices $\mathbf{F}$ and $\mathbf{G}$ [Becker and Teschner 2007]:

By introducing the two parameters

$$\lambda = \frac{E}{(1+\nu)(1-2\nu)} \tag{3.36}$$

and

$$\alpha = \lambda\nu \tag{3.37}$$

Equation 3.32 can be written as

$$\mathbf{E} = \lambda\mathbf{F} + \alpha\mathbf{G} \tag{3.38}$$

The parameter α is also known as Lamé's constant in elasticity theory whereas λ is not directly related to any elasticity constant.

As we will see in Chapter 5, this parameterization has several advantages: It will allow us to formulate the parameter fitting as a linear system of equations. Furthermore, potential numerical problems caused by Poisson ratios near the singularities -1 or 0.5 are avoided.

We conclude this section by summarizing the conversion formulas for the two pairs of isotropic constants:

The conversions from (λ, α) to (ν, E) are

$$\nu = \frac{\alpha}{\lambda} \tag{3.39}$$

and

$$E = \lambda(1+\nu)(1-2\nu) \tag{3.40}$$

And the inverse conversions are

$$\lambda = \frac{E}{(1+\nu)(1-2\nu)} \tag{3.41}$$

and

$$\alpha = \nu\lambda \tag{3.42}$$

3.3 Warped Stiffnesses

As mentioned before, the linear Cauchy strain, as defined in Equation 3.2, is not rotational-invariant. This may lead to significant linearization artifacts in case of large rotational deformations. Those artifacts can effectively be avoided by using warped stiffnesses [Müller et al. 2002, Müller and Gross 2004]. The basic idea is to compute the elastic forces that act at the nodes of an element in an unrotated frame before rotating them back to the frame of the deformed element. To this end, rotation matrices between deformed and undeformed element frames have to be computed. However, those can only be calculated if the three-dimensional coordinates of all of the involved nodes are known. The problem is now that it is extremely difficult to measure the displacements of nodes in the interior of an object. We therefore assume a one-layer material where we only have nodes on the object's surface. We will discuss these simplifications in Subsection 3.3.1. Thereafter, the warped stiffness approach will be discussed in more detail. We conclude this Section with a derivation of a new set of algebraic equations for our specific problem.

3.3.1 One-Layer Material

In Subsection 3.1.7, we derived the following reduce equation system:

$$\begin{bmatrix} \mathbf{K}_{\partial\Omega_f,\partial\Omega_f} & \mathbf{K}_{\partial\Omega_f,\Omega} \\ \mathbf{K}_{\Omega,\partial\Omega_f} & \mathbf{K}_{\Omega,\Omega} \end{bmatrix} \begin{bmatrix} \mathbf{u}_{\partial\Omega_f} \\ \mathbf{u}_{\Omega} \end{bmatrix} = \begin{bmatrix} \mathbf{f}_{\partial\Omega_f} \\ \mathbf{o} \end{bmatrix} \tag{3.43}$$

If we assume a one-layer material, we do not have nodes in the body's interior ($\Omega \setminus \partial\Omega$) and the above equation system can be further reduced to:

$$\mathbf{K}_{\partial\Omega_f,\partial\Omega_f}\mathbf{u}_{\partial\Omega_f} = \mathbf{f}_{\partial\Omega_f} \tag{3.44}$$

In the following $\mathbf{Ku} = \mathbf{f}$ stands for this reduces equation system if not mentioned otherwise.

3.3.2 Element-Based Warped Stiffnesses

The global displacement vector $\mathbf{u}$ in the equation system $\mathbf{Ku} = \mathbf{f}$ can be expressed as the difference of the global vector of nodal absolute positions, denoted as $\mathbf{x}$, and the global vector of initial nodal positions, denoted as $\mathbf{x}_0$. Our equation system can therefore be written as:

$$\mathbf{K}(\mathbf{x} - \mathbf{x}_0) = \mathbf{f} \tag{3.45}$$

If we zoom in to one element e, this equation translates to:

$$\mathbf{K}_e(\mathbf{x}_e - \mathbf{x}_{0e}) = \mathbf{f}_e \tag{3.46}$$

where $\mathbf{K}_e$ now denotes the element stiffness, $\mathbf{x}_e$ and $\mathbf{x}_{0e}$ the 12×1 vectors of absolute and initial node positions and $\mathbf{f}_e$ the 12×1 vector that collects the forces acting at the four nodes of e.

The essential idea of the warped stiffnesses is now as follows (see Figure 3.3 for an illustration):

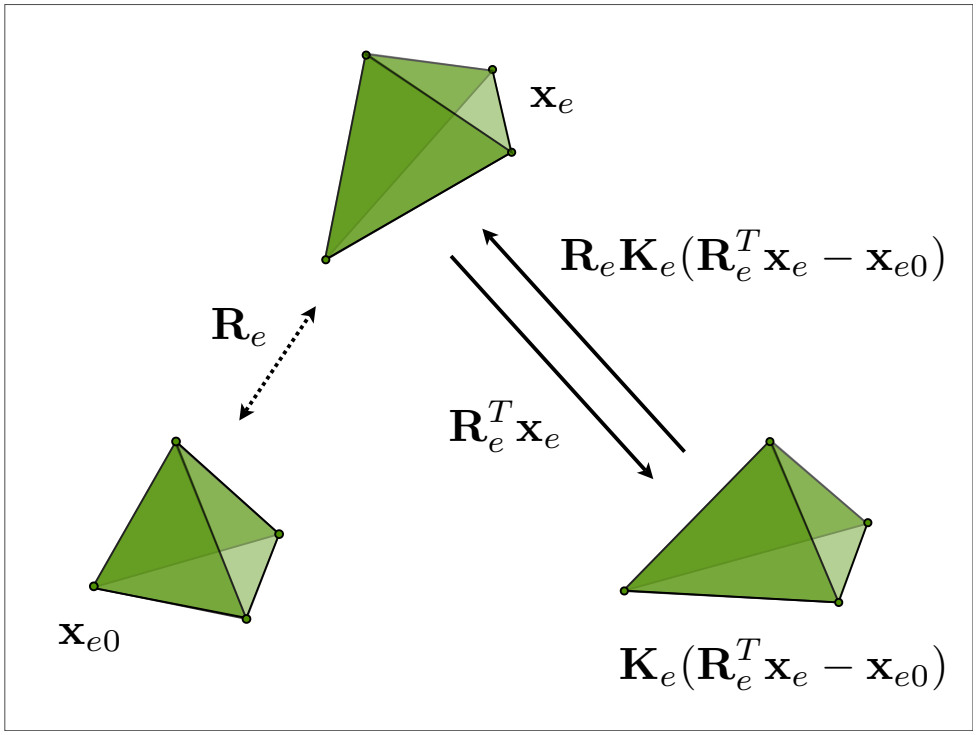

Figure 3.3: *Stiffness Warping.*

Let us assume that we know the matrix $\mathbf{Z}_e$, which describes the rotation from the undeformed element frame to its deformed frame. We will discuss its computation from the vectors $\mathbf{x}_e$ and $\mathbf{x}_{0e}$ in the next Subsection. If we construct a 12×12 matrix $\mathbf{R}_e$ with four $\mathbf{Z}_e$ matrices on its diagonal

$$\mathbf{R}_e = \begin{bmatrix} \mathbf{Z}_e & & & \\ & \mathbf{Z}_e & & \\ & & \mathbf{Z}_e & \\ & & & \mathbf{Z}_e \end{bmatrix} \tag{3.47}$$

we can simultaneously transform all the node positions of the deformed element e to the unrotated frame by computing:

$$\mathbf{R}_e^T \mathbf{x}_e \tag{3.48}$$

This allows us to compute the unrotated element strain as:

$$\varepsilon_e = \mathbf{B}_e(\mathbf{R}_e^T \mathbf{x}_e - \mathbf{x}_{0e}) \tag{3.49}$$

The forces acting at the nodes in the unrotated frame can therefore be computed by multiplying the displacement vector $\mathbf{R}_e^T \mathbf{x}_e - \mathbf{x}_{0e}$ with the element's stiffness matrix $\mathbf{K}_e$. This expression is finally rotated back to get the four forces acting on the nodes of the deformed element. This whole procedure can be summarized as:

$$\mathbf{R}_e \mathbf{K}_e \left(\mathbf{R}_e^T \mathbf{x}_e - \mathbf{x}_{0e}\right) = \mathbf{f}_e \tag{3.50}$$

or

$$\mathbf{R}_e \mathbf{K}_e \mathbf{R}_e^T \mathbf{x}_e - \mathbf{R}_e \mathbf{K}_e \mathbf{x}_{0e} = \mathbf{f}_e \tag{3.51}$$

By zooming out again, we see that our new system of equations is basically given by:

$$\mathbf{K}'\mathbf{x} - \mathbf{K}''\mathbf{x_0} = \mathbf{f} \tag{3.52}$$

with the two stiffness matrices

$$\mathbf{K}' = \sum_e \mathbf{R}_e \mathbf{K}_e \mathbf{R}_e^T \tag{3.53}$$

and

$$\mathbf{K}'' = \sum_e \mathbf{R}_e \mathbf{K}_e \tag{3.54}$$

We get the displacement vector $\mathbf{u}$ by solving the system 3.52 for $\mathbf{x}$ and computing $\mathbf{u} = \mathbf{x} - \mathbf{x}_0$.

3.3.3 Rotation Matrices

In the last Subsection we assumed that the rotation matrices $\mathbf{Z}_e$ are known. We will now discuss how to compute them using the deformed $\mathbf{x}_e$ and undeformed nodes $\mathbf{x}_{0e}$. Let us assume that the global node indices of element e are denoted as i, j, k, l so that the deformed nodes can be expressed as $\mathbf{x}_e = \left[\mathbf{x}_e^i, \mathbf{x}_e^j, \mathbf{x}_e^k, \mathbf{x}_e^l\right]^T$ and undeformed nodes as $\mathbf{x}_{0e} = \left[\mathbf{x}_{0e}^i, \mathbf{x}_{0e}^j, \mathbf{x}_{0e}^k, \mathbf{x}_{0e}^l\right]^T$. The rotation matrix $\mathbf{Z}_e$ can then be computed as follows:

1. Construct the two matrices

$$\mathbf{X}_{0,e} = \begin{bmatrix} \mathbf{x}_{0e}^i & \mathbf{x}_{0e}^j & \mathbf{x}_{0e}^k & \mathbf{x}_{0e}^l \\ 1.0 & 1.0 & 1.0 & 1.0 \end{bmatrix} \tag{3.55}$$

and

$$\mathbf{X}_e = \begin{bmatrix} \mathbf{x}_e^i & \mathbf{x}_e^j & \mathbf{x}_e^k & \mathbf{x}_e^l \\ 1.0 & 1.0 & 1.0 & 1.0 \end{bmatrix} \tag{3.56}$$

from the deformed and undeformed nodal positions.

2. Compute the following matrix:

$$\mathbf{X}_e \mathbf{X}_{0,e}^{-1} = \begin{bmatrix} \mathbf{Y}_e & \mathbf{t}_e \\ \mathbf{o}^T & 1.0 \end{bmatrix} \tag{3.57}$$

3. Apply a singular value decomposition (SVD) to the upper left block matrix $\mathbf{Y_e}$:

$$\mathbf{Y}_e = \mathbf{U}_e^T \mathbf{\Sigma}_e \mathbf{V}_e \tag{3.58}$$

4. Compute the element rotation matrix as $\mathbf{Z}_e = \mathbf{U}_e^T \mathbf{V}_e$. (Note that the columns in $\mathbf{Z}_e$ have to be normalized!)

3.4 A More Flexible FEM Approximation

The FEM approximation we discussed so far is not flexible enough to approximate the deformation behavior of a general deformable object. The reason for that is that we assumed a homogenous, isotropic Hookean material. In this Section, we therefore refine our linear constitutive Equation 3.18 to an element-wise linear stress-strain relation. Thereafter, our final parameterization based on isotropic elements is introduced and the new element stiffness matrices are discussed. We conclude by introducing our final system of algebraic equations.

3.4.1 Element-Wise Linear Stress-Strain Relation

In Subsection 3.1.3 we assumed a material that follows Hooke's law of elasticity. On the level of an element this linear strain-stress relation is given by:

$$\sigma_e = \mathbf{E} \varepsilon_e \tag{3.59}$$

where the matrix $\mathbf{E}$ is assumed to be the same for all elements e.

We refine this assumption and assume an element-wise linear stress-strain relation. In other words, we assume the matrix $\mathbf{E}$ to be different for all elements e. The discretized constitutive equation for element e is therefore:

$$\sigma_e = \mathbf{E}_e \varepsilon_e \tag{3.60}$$

This element-wise Hookean material allows us to better approximate inhomogeneous material behavior.

3.4.2 Isotropic Elements

However, there are to many degrees of freedom if a general element-wise linear material is assumed and our parameter fitting would get infeasible. We therefore assume an element-wise

isotropic material. In other words, we define the matrix $\mathbf{E}_e$ to be (compare with the derivation in Subsection 3.2):

$$\mathbf{E}_e = \lambda_e \mathbf{F} + \alpha_e \mathbf{G} \tag{3.61}$$

with the two isotropic elasticity constants λ_e and α_e.

This formulation still allows to approximate anisotropic material behavior to some degree because the isotropic materials are defined on a per-element basis.

Hence, the final parameterization based on *element-wise isotropic tetrahedra* allows us to approximate linear inhomogeneous, *pseudo-anisotropic* material behavior

3.4.3 Stiffness Matrices

As we saw in the derivation of the discrete equilibrium equation in Subsection 3.1.6, the element stiffness matrices can be computed as:

$$\mathbf{K}_e = V_e \mathbf{B}_e^T \mathbf{E} \mathbf{B}_e \tag{3.62}$$

In case of an element-wise isotropic material, where we have an element dependent matrix $\mathbf{E}_e$ we get:

$$\mathbf{K}_e = V_e \mathbf{B}_e^T \mathbf{E}_e \mathbf{B}_e = \lambda_e V_e \mathbf{B}_e^T \mathbf{F} \mathbf{B}_e + \alpha_e V_e \mathbf{B}_e^T \mathbf{G} \mathbf{B}_e = \lambda_e \mathbf{C}_e + \alpha_e \mathbf{D}_e \tag{3.63}$$

where $\mathbf{C}_e = V_e \mathbf{B}_e^T \mathbf{F} \mathbf{B}_e$ and $\mathbf{D}_e = V_e \mathbf{B}_e^T \mathbf{G} \mathbf{B}_e$.

We get our final equation system by using these new element stiffnesses in the construction of the two global stiffness matrices $\mathbf{K}'$ and K":

If we introduce a global parameter vector $\mathbf{p} = [\ldots, \lambda_e, \ldots | \ldots, \alpha_e, \ldots]^T$ and local parameter vectors $\mathbf{p}_e = [\lambda_e, \alpha_e]^T$, we can summarize our system as:

$$\mathbf{K}'(\mathbf{p})\mathbf{x} - \mathbf{K}''(\mathbf{p})\mathbf{x}_0 = \mathbf{f} \tag{3.64}$$

with the unknown vector $\mathbf{x}$ and the two stiffness matrices

$$\mathbf{K}'(\mathbf{p}) = \sum_e \mathbf{R}_e \mathbf{K}_e(\mathbf{p}_e) \mathbf{R}_e^T \tag{3.65}$$

and

$$\mathbf{K}''(\mathbf{p}) = \sum_e \mathbf{R}_e \mathbf{K}_e(\mathbf{p}_e) \mathbf{R}_e^T \tag{3.66}$$

Note that we can get the system for a homogenous isotropic material by simply replacing the local parameter vectors by $\mathbf{p}_e = [\lambda, \alpha]^T$.

4

Measuring Contact Interactions

The major subject of this Chapter is the system we developed to acquire the kinds of *contact measurements* we need to fit our model parameters. The development of such an acquisition system is a critical step because all subsequent results depend on the quality of the measurements we can acquire. The key challenge involved in building such a system is that contact measurements cannot simply be observed but must be *excited* by a physical interaction with the object. This, in turn, may lead to *occlusions* during the acquisition process. In spite of the importance of the acquisition system we keep its description rather short as it is not the main focus of this work. We start with a disquisition on our system and its individual components. In Section 4.2, we briefly discuss the processing steps needed to obtain actual measurements from the acquired data. We conclude by introducing a mathematical notation for our measured contact interactions.

4.1 Acquisition System

The static deformation responses that are needed to estimate our model parameters consist of *surface displacements* and corresponding *contact forces*. Our acquisition system is thus composed of two major components: A *trinocular stereo vision system* to acquire the surface deformation and *force sensors* to measure the corresponding forces.

Trinocular Stereo Vision System Figure 4.1 shows our trinocular stereo vision system which consists of three Canon 40D cameras that capture images at a resolution of 3888×2592. These cameras are placed in a triangular configuration to minimize occlusions caused by the *contact probes* during the data acquisition. We also built an external trigger device to synchronize the triggering of the three cameras and integrated two light sources to ensure a uniform illumination

during the acquisition process.

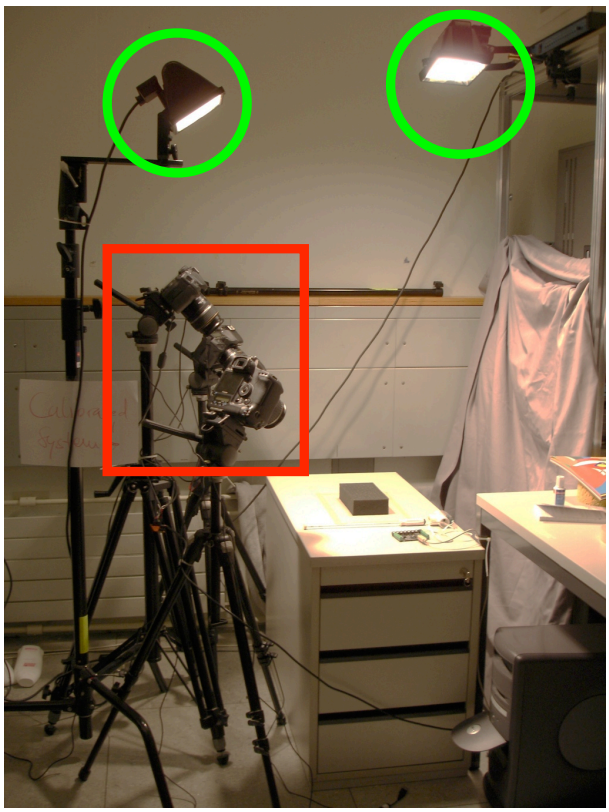

Figure 4.1: *Our trinocular stereo vision system consists of three high-resolution cameras (indicated by a red rectangle) and two light sources (indicated by green circles). The cameras are arranged in a triangular setup. This arrangement helps to maximize the visibility during the capturing of a contact interaction. The light sources make sure that the object is uniformly illuminated during the acquisition.*

The surface displacement of a static deformation response is measured by using a set of *markers* that we paint on the object's visible surface. Figure 4.2 illustrates the process of spray-painting a sponge using four different colors. The 180 markers were painted on a regular grid to simplify the later registration. However, this is not required in general. Our system is capable of measuring viewpoint-registered marker positions to an accuracy of approximately 1 mm.

For the physical interactions we built contact probes with circular disks of different diameters attached to the tip of an extra long, white-painted screwdriver. The position and orientation of the contact probe is estimated using two makers on the shaft of the screwdriver.

Force Sensors To measure contact forces, we integrated *force sensing resistors* (FSR) in our contact probes. We use the FSR Phidget Sensor Kit developed by Trossen Robotics[1] to control these sensing resistors. The force sensors allow use to measure force magnitudes of contacts during the acquisition process. Furthermore, we synchronized the force sensor's read operation with the camera trigger signal. A contact probe with integrated force sensor is shown in Figure 4.3.

[1] http://www.trossenrobotics.com

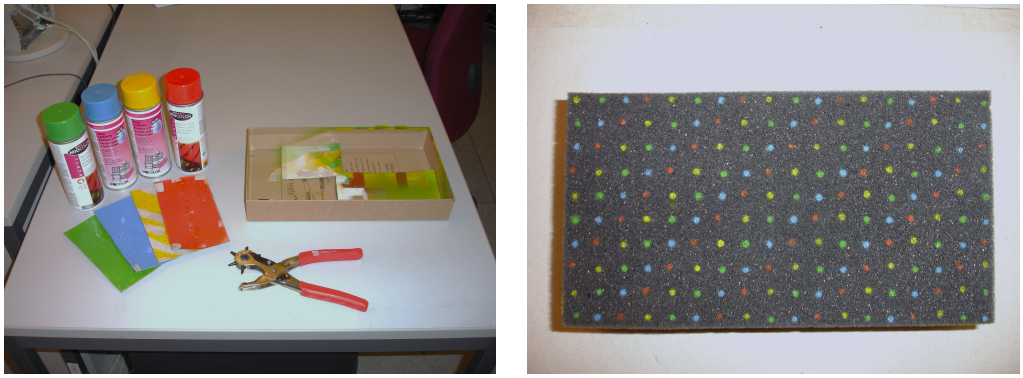

(a) (b)

Figure 4.2: *Painting a sponge.* (a) *Aerosol cans and templates used to paint colored markers on a sponge.* (b) *Sponge with colored markers.*

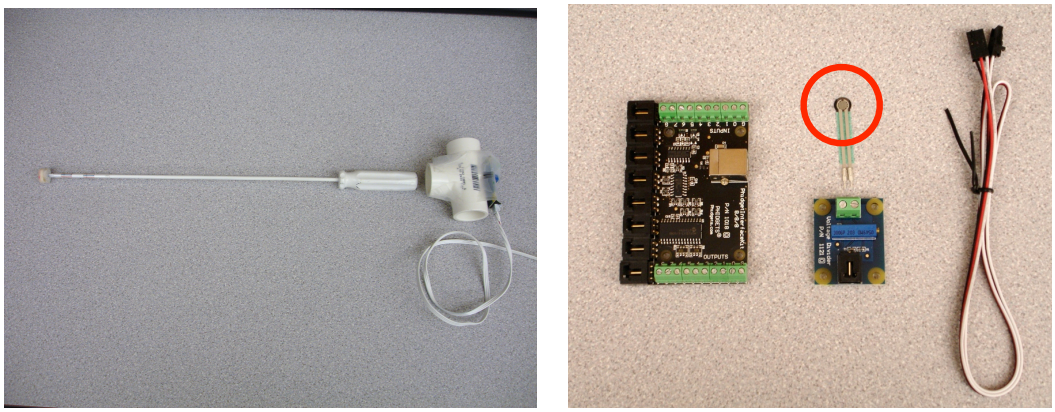

(a) (b)

Figure 4.3: *Contact probe.* (a) *Contact probe with integrated force sensor.* (b) *Force sensing resistor (red circle).*

4.2 Processing Steps

In the last Section, we saw how contact interactions can be acquired. In this Section, we will discuss the necessary processing steps to obtain actual measurements from the acquired data.

The first step is to extract markers from the captured images. To this end, we use simple thresholding in the CIELab color space followed by a correction step using morphological operations. We do that for all the different marker colors independently. This procedure, even though simple, allows for a robust extraction of the markers.

In a second step, the marker positions have to be reconstructed in 3d. Accurate depth estimation relies on finding markers between the calibrated stereo cameras [Bouguet 2006]. For this purpose, the makers in the individual frames are labeled and correspondences are established. A marker can be reconstructed if it is visible in at least two of the three camera images. These reconstructed makers are then registered to a template mesh using a modified version of Horn's shape matching algorithm [Micheals and Boult 2000]. Even though the use of three cameras reduces the number of occluded markers noticeably, occasional occlusions can not be avoided. We therefore employ the linear shell-based approach [Bickel et al. 2007] in our work which incorporates the prescribed displacements (visible markers) as boundary constraints, and, otherwise, minimizes surface stretching and bending to estimate the displacement of the occluded markers. As a result, we get a complete reconstruction of makers that describe the surface deformation of a measured contact interaction.

As mentioned before, we estimate the position and orientation of a contact probe by using two makers on the shaft of the screwdriver. The contact magnitude is measured by using a calibrated FSR integrated at the top of the handle of the contact probe. For the calibration of the force sensors, we simply use a balance and Newton's second law of motion. The calibration procedure is illustrated in Figure 4.4. We use our data acquisition system with its synchronized image and force sensors to capture a set of images and corresponding FSR values while we poke the balance with the to-be-calibrated contact probe (see Figure 4.4 (a)). The output of this procedure is a set of sensor values v with corresponding weight values m. The weight values are then converted to force values by multiplying the individual m's with the gravitational constant g. This allows us to fit a sensor response curve (see Figure 4.4 (b)) to the set of sensor-value-force-pairs. Force magnitudes (in N) can then be calculated by simply evaluating the fitted response curve.

4.3 A Notation for Measured Contact Interactions

In the next Chapter, we will substitute measured displacements and corresponding forces into the governing finite element equations to formulate our inverse problem. To this end, we introduce a mathematical notation for our measured contact interactions here:

Deformation measurements record surface displacements and corresponding contact forces. We denote the measured surface displacements as $\bar{\mathbf{u}}$ and the corresponding contact forces as $\bar{\mathbf{f}}$. However, it is often more convenient to use absolute positions of nodes instead of their displacements. A second notation is therefore given by the pair: $(\bar{\mathbf{x}}, \bar{\mathbf{f}})$ where $\bar{\mathbf{x}}$ denotes the vector

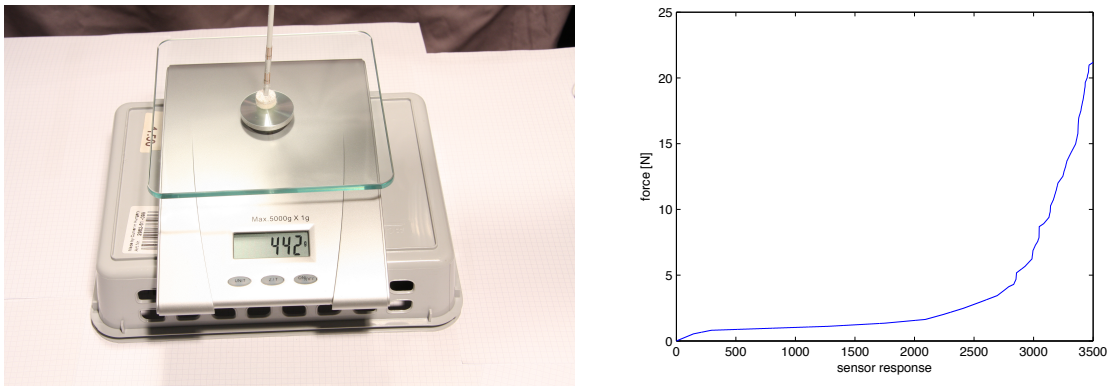

(a) (b)

Figure 4.4: *Force sensor calibration.* (a) *An image of the balance showing the "weight" of an applied contact force.* (b) *Fitted sensor response curve for a typical FSR.*

of measured nodal absolute positions. If multiple measurements are used together we indicate that by using a subscript i for the i-th measurement.

Let us summarize: The notation $(\bar{\mathbf{x}}, \bar{\mathbf{f}})$ or $(\bar{\mathbf{u}}, \bar{\mathbf{f}})$ is used for individual measurements and the notation $(\bar{\mathbf{x}}_i, \bar{\mathbf{f}}_i)$ or $(\bar{\mathbf{u}}_i, \bar{\mathbf{f}}_i)$ is used if multiple measurements are involved.

A set of acquired contact interactions of the sponge are summarized in Figure 4.5.

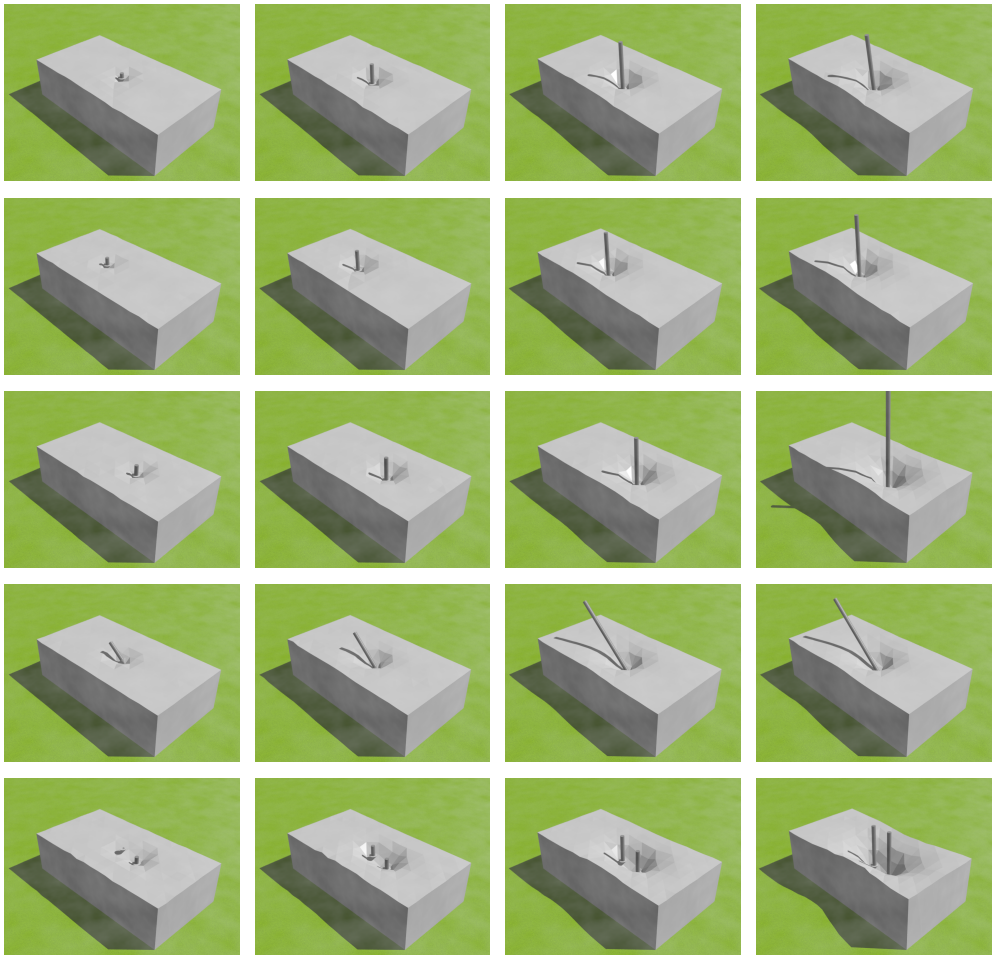

Figure 4.5: *Set of example deformations of the sponge.*

5

Inverse Analysis of Contact Interactions

An *inverse problem* is a problem where the values of some model parameters must be obtained from observed data. In our context, the observed data consists of measured contact interactions and the model parameters are a set of inhomogeneous material properties. In other words, we are trying to estimate a set of spatially varying material parameters of an object by using observations on its surface only. Our problem is therefore *ill-posed*. In Chapter 3, we used direct analysis to derive the set of governing finite equations that allows us to compute the deformation response of a general object upon contact. If we substitute our measured contact interactions into these finite set of equations we are able to formulate two different *discrete inverse problems* with the material parameters as its unknowns: A *linear* inverse problem that allows us to estimate the material parameters by minimizing a *force-based energy* and a *non-linear* inverse problem where the parameters are fitted by minimizing a *displacement-based* energy. Discrete inverse problems, as opposed to their continuous counterparts, might not only be ill-posed but also *ill-conditioned*. The *theory of regularization* provides powerful techniques to solve such discrete inverse problems by adding proper *smoothness constraints*, resulting in a well-posed problem. We employ two kinds of constraints in our problem formulations: The first kind enforces fitted parameters to be smoothness over *neighboring elements* in *individual* fitted contact interactions and the second enforces the parameters to be smooth over *corresponding elements* in *all* the fitted interactions.

Before we start with the inverse analysis of our specific problem, we will clarify some important notions and briefly review the general linear and non-linear inverse formulations. In the two subsequent Sections, our force- and displacement-based inverse problems are formulated.

5.1 Linear and Non-linear Inverse Problems

According to Hadamard[1], a problem is *well-posed* if it fulfills the following three conditions:

1. *Existence*: A solution always exists.
2. *Uniqueness*: The solution is unique.
3. *Continuity*: If the error in the input is small, the induced error in in the solution is small as well.

Ill-posed problems, as opposed to well-posed problems, are extremely hard because non of the above conditions are necessarily satisfied: If a problem is under-constraint, as ill-posed problems typically are, solutions are usually ambiguous or might even not exist.

The third of the above conditions is also an extremely important property because it is directly related to the *stability* and *robustness* of a solution. It determines what the *effect of noise*, inherent in all physical measurements, might have on our solution.

In case of a discrete problem it could even get worse because even if it is well-posed, it might still be ill-conditioned. Ill-conditioning itself might lead to potentially very sensitive solutions if the input data is perturbated.

The theory of regularization provides powerful tools to improve the posedness and also the condition of a general inverse problem by incorporating further information about the desired solution.

In the following we briefly review the general formulations of linear and non-linear inverse problems before we start with the derivations of our domain-specific formulations:

Linear Inverse Problem

A smooth and stable solution $\hat{\mathbf{x}}$ of an underdetermined linear system of equations

$$\mathbf{A}\mathbf{x} = \mathbf{b} \tag{5.1}$$

can be computed by introducing a constraint matrix $\mathbf{L}$ that approximates, for instance, the first derivative operator and by minimizing the following weighted combination of the system's residual and the smoothness constraints:

$$\hat{\mathbf{x}} = \arg\min_{\mathbf{x}} \left\{ ||\mathbf{A}\mathbf{x} - \mathbf{b}||_2^2 + \gamma^2 ||\mathbf{L}\mathbf{x}||_2^2 \right\} \tag{5.2}$$

with a weight γ, which we call regularization parameter, that controls the amount of regularization.

The solution $\hat{\mathbf{x}}$ of 5.2 can be found by solving the equation system

$$\begin{bmatrix} \mathbf{A} \\ \gamma\mathbf{L} \end{bmatrix} \mathbf{x} = \begin{bmatrix} \mathbf{b} \\ \mathbf{o} \end{bmatrix} \tag{5.3}$$

in a least squares sense.

[1] Jacques Salomon Hadamard, French mathematician, 1865-1963

Non-Linear Inverse Problem

In case of an underdetermined system of non-linear equations

$$F(\mathbf{x}) = \mathbf{y} \tag{5.4}$$

with $F : \mathbb{R}^n \rightarrow \mathbb{R}^m$ and $n > m$, a smooth and stable solution $\hat{\mathbf{x}}$ can be found by solving:

$$\hat{\mathbf{x}} = \arg\min_{\mathbf{x}} \left\{ ||F(\mathbf{x}) - \mathbf{y}||_2^2 + \gamma^2 ||\mathbf{L}\mathbf{x}||_2^2 \right\} \tag{5.5}$$

where γ denotes the regularization parameter and $\mathbf{L}$ the constraint matrix.

If we introduce a vector-valued function

$$G(\mathbf{x}) = \begin{bmatrix} F(\mathbf{x}) - \mathbf{y} \\ \gamma \mathbf{L}\mathbf{x} \end{bmatrix} \tag{5.6}$$

we can recast 5.5 as a non-linear least squares problem:

$$\hat{\mathbf{x}} = \arg\min_{\mathbf{x}} ||G(\mathbf{x})||_2^2 \tag{5.7}$$

Non-linear least squares solvers often take the vector-valued function $G(\mathbf{x})$ and, optionally, its Jacobian

$$J_G(\mathbf{x}) = \begin{bmatrix} J_F(\mathbf{x}) \\ \gamma \mathbf{L} \end{bmatrix} \tag{5.8}$$

as an input. $J_F(\mathbf{x})$ denotes the Jacobian of $F(\mathbf{x})$.

The Influence of the Regularization Parameter γ

The influence of the regularization parameter γ is illustrated in Figure 5.1. Note that one must give up the requirement of the residual norm to be zero. In our case, however, this is a desired property to prevent overfitting and allows the model to generalize beyond the (potentially) noisy) fitting data. We are instead seeking a solution $\hat{\mathbf{x}}$ that provides a good tradeoff between a minimal residual norm and a minimal norm of the regularization term $\mathbf{L}\mathbf{x}$. The amount of regularization can be controlled by γ and the dependencies can be summarized in formulas as:

$$\gamma \rightarrow \infty \text{ implies } ||\mathbf{L}\mathbf{x}||_2 \rightarrow 0 \text{ and } ||\mathbf{A}\mathbf{x} - \mathbf{b}||_2 \rightarrow \infty \text{ or } ||F(\mathbf{x}) - \mathbf{y}||_2 \rightarrow \infty. \tag{5.9}$$

and

$$\gamma \rightarrow 0 \text{ implies } ||\mathbf{L}\mathbf{x}||_2 \rightarrow \infty \text{ and } ||\mathbf{A}\mathbf{x} - \mathbf{b}||_2 \rightarrow 0 \text{ or } ||F(\mathbf{x}) - \mathbf{y}||_2 \rightarrow 0. \tag{5.10}$$

In words: Increasing the regularization parameter γ leads to smoother solutions $\hat{\mathbf{x}}$ but also to an increase of the residual norm. On the other hand, if the regularization parameter is decreased the residual gets smaller but the resulting solution is less smooth.

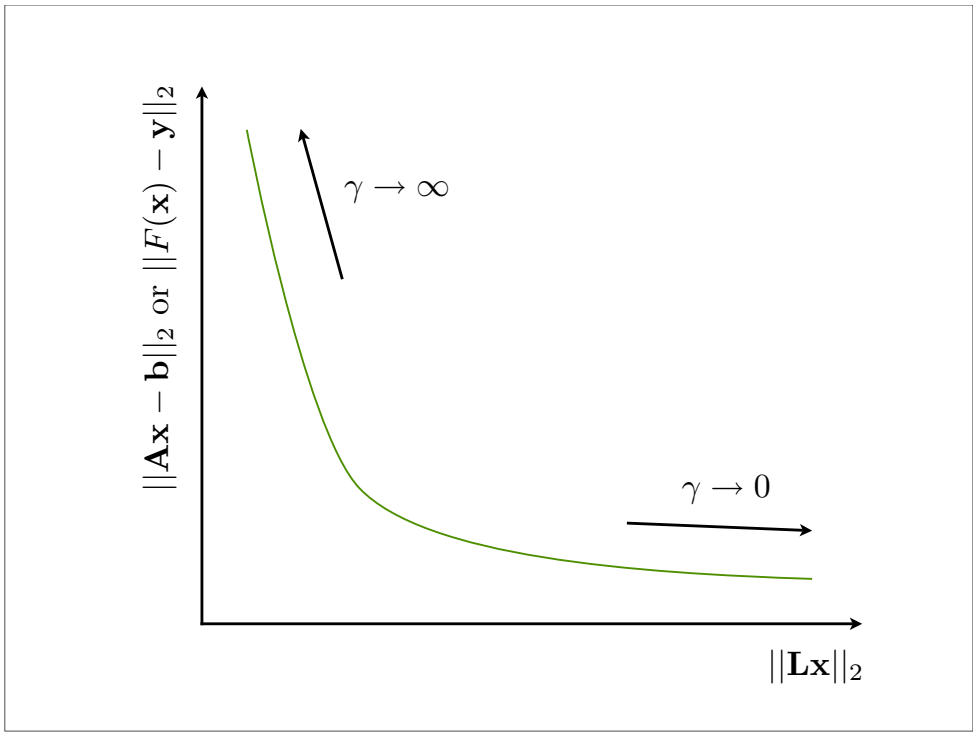

Figure 5.1: *Influence of the regularization parameter γ.*

5.2 Force-Based Inverse Analysis

The subject of this Section is a force-based inverse analysis of general contact interactions, whose direct analysis was performed in Chapter 3. In contrast to a displacement-based analysis, a force-based approach allows us to formulate our problem as a *linear* inverse problem. In the next Subsection, we will start our discussion by analyzing an individual interaction. The resulting parameter estimation is then extended in Subsection 5.2.2 so that material parameters of multiple interactions can be fitted simultaneously. This extension allows us to enforce smoothness of parameters over multiple fits, which turns out to be very useful for the smooth blending of fitted interactions in following Chapter 6.

5.2.1 Inverse Analysis of an Individual Contact Interaction

In Chapter 3, we derived a finite set of equations that allows us to compute the deformation response of a deformable object on a specific contact by assuming that the material properties are known. In this Section, we will inversely use these equations to derive a linear force-based inverse problem which allows us to estimate the material parameters by incorporating acquired contact interactions from Chapter 4.

For the convenience of the reader, we repeat the result of the direct analysis here:

Let $\mathbf{p} = [\ldots, \lambda_e, \ldots | \ldots, \alpha_e, \ldots]^T$ denote the vector of all element-wise isotropic material parameters and $\mathbf{p}_e = [\lambda_e, \alpha_e]^T$ the vector of the parameters of an individual element. The result of the direct analysis is the following system of equations that can be use to compute the

deformation response $\mathbf{x}$ on a specific contact $\mathbf{f}$:

$$\mathbf{K}'(\mathbf{p})\mathbf{x} - \mathbf{K}''(\mathbf{p})\mathbf{x_0} = \mathbf{f} \tag{5.11}$$

with stiffness matrices

$$\mathbf{K}'(\mathbf{p}) = \sum_e \mathbf{R}_e \mathbf{K}_e(\mathbf{p}_e)\mathbf{R}_e^T \tag{5.12}$$

and

$$\mathbf{K}''(\mathbf{p}) = \sum_e \mathbf{R}_e \mathbf{K}_e(\mathbf{p}_e) \tag{5.13}$$

and element stiffnesses

$$\mathbf{K}_e(\mathbf{p}_e) = \mathbf{K}_e(\lambda_e, \alpha_e) = \lambda_e \mathbf{C}_e + \alpha_e \mathbf{D}_e \tag{5.14}$$

By substituting a measured contact interaction $(\bar{\mathbf{x}}, \bar{\mathbf{f}})$ in the equation system 5.11, it can be reformulated so that the parameter vector $\mathbf{p}$ is the unknown of a linear system of equations $\mathbf{A}(\bar{\mathbf{x}})\mathbf{p} = \bar{\mathbf{f}}$:

The substitution of a measured interaction leads to:

$$\left[\sum_e \lambda_e \mathbf{R}_e \mathbf{C}_e \mathbf{R}_e^T + \sum_e \alpha_e \mathbf{R}_e \mathbf{D}_e \mathbf{R}_e^T\right] \bar{\mathbf{x}} - \left[\sum_e \lambda_e \mathbf{R}_e \mathbf{C}_e + \sum_e \alpha_e \mathbf{R}_e \mathbf{D}_e\right] \mathbf{x}_0 = \bar{\mathbf{f}} \tag{5.15}$$

If we break the global vectors $\bar{\mathbf{x}}$ and $\mathbf{x}_0$ into 12×1 element vectors $\bar{\mathbf{x}}_e$ and $\mathbf{x}_{0e}$, we can reformulate the above system as

$$\sum_e \left[\lambda_e \left[\mathbf{R}_e \mathbf{C}_e \mathbf{R}_e^T \bar{\mathbf{x}}_e - \mathbf{R}_e \mathbf{C}_e \mathbf{x}_{0e}\right] + \alpha_e \left[\mathbf{R}_e \mathbf{D}_e \mathbf{R}_e^T \bar{\mathbf{x}}_e - \mathbf{R}_e \mathbf{D}_e \mathbf{x}_{0e}\right]\right] = \bar{\mathbf{f}} \tag{5.16}$$

and realize that we can write the global force vector $\bar{\mathbf{f}}$ as a linear combination of element vectors $\mathbf{s}_e$ and $\mathbf{t}_e$:

$$\sum_e \left[\lambda_e \mathbf{s}_e + \alpha_e \mathbf{t}_e\right] = \bar{\mathbf{f}} \tag{5.17}$$

where

$$\mathbf{s}_e = \mathbf{R}_e \mathbf{C}_e \mathbf{R}_e^T \bar{\mathbf{x}}_e - \mathbf{R}_e \mathbf{C}_e \mathbf{x}_{0e} \tag{5.18}$$

and

$$\mathbf{t}_e = \mathbf{R}_e \mathbf{D}_e \mathbf{R}_e^T \bar{\mathbf{x}}_e - \mathbf{R}_e \mathbf{D}_e \mathbf{x}_{0e} \tag{5.19}$$

Note that we used $\sum_e$ as a sum over element vectors instead of element matrices here. This is simply a one dimensional version of the matrix assembly procedure described in Subsection 3.1.8.

If we convert the vectors $\mathbf{s}_e$ and $\mathbf{t}_e$ to vectors of global size and collect them column-wise in matrices $\mathbf{S}$ and $\mathbf{T}$, we get our final linear system of equations with the parameter vector as its unknown:

$$[\mathbf{S}|\mathbf{T}]\,\mathbf{p} = \mathbf{A}(\bar{\mathbf{x}})\mathbf{p} = \bar{\mathbf{f}} \tag{5.20}$$

with

$$\mathbf{A}(\bar{\mathbf{x}}) = [\mathbf{S}|\mathbf{T}] \tag{5.21}$$

Note that the matrix $\mathbf{A}(\bar{\mathbf{x}})$ is dependent on the measured deformation response $\bar{\mathbf{x}}$.

The equation system 5.20 is extremely sparse, but in general underdetermined. Its dimensions are $3u \times 2t$ if u denotes the number of unconstrained nodes (nodes minus geometric constraints) and t the number of elements e.

The next step is therefore to introduce proper smoothness constraints.

Enforcing Spatial Smoothness

The system $\mathbf{A}(\bar{\mathbf{x}})\mathbf{p} = \bar{\mathbf{f}}$ is under-constrained and has, in general, infinitely many solutions for a measured contact interaction $(\bar{\mathbf{x}}, \bar{\mathbf{f}})$. Hence, further information about the material properties have to be incorporated. A reasonable assumption seems to be that the material properties of an object with an inhomogeneous behavior are smoothly changing across its body. This observation can be incorporated into our discrete formulation by forcing parameters of neighboring elements to be smooth:

We have two different kinds of material parameters, namely λ_e's and α_e's, in our model. In Subsection 3.4.3, we defined $\mathbf{p}$ to be the vector that collects *all* of the parameters:

$$\mathbf{p} = [\ldots, \lambda_e, \ldots | \ldots, \alpha_e, \ldots]^T \tag{5.22}$$

For the sake of clarity, we split the parameter vector $\mathbf{p}$ into two vectors $\mathbf{l}$ and $\mathbf{a}$ here:

$$\mathbf{l} = [\ldots, \lambda_e, \ldots] \tag{5.23}$$

and

$$\mathbf{a} = [\ldots, \alpha_e, \ldots] \tag{5.24}$$

Let us now derive the constraint matrix $\mathbf{L}_s$ that enforces the above-mentioned *spatial smoothness* of our parameters. Note that constraint equations are only dependent on the finite element discretization (geometry) and not on the kind of parameter. We therefore concentrate on the λ_e's in the following but the resulting constraint matrix can also be used to enforce spatial smoothness of the α_e's:

Let us assume that e and e' are a pair of neighboring elements as illustrated in Figure 5.2. The parameter vector $\mathbf{l}$, in which the corresponding element parameters are highlighted, is given as:

$$\mathbf{l} = [\ldots, \lambda_e, \ldots, \lambda_{e'}, \ldots] \tag{5.25}$$

Our goal is now to formulate a constraint equation so that the difference between the parameter values $\lambda_e - \lambda_{e'}$ goes to zero if the regularization parameter goes to infinity. To this end, we construct a row vector of the same size as our parameter vector $\mathbf{l}$ that has a 1 at index e and a -1 at index e' and is zero otherwise, and we get the constraint equation by setting the inner product of this vector and the parameter vector $\mathbf{l}$ to zero.

The constraint matrix can therefore be constructed by repeating the above procedure for all the neighboring element pairs (e, e') and collecting the rows in a matrix $\mathbf{L}_s$.

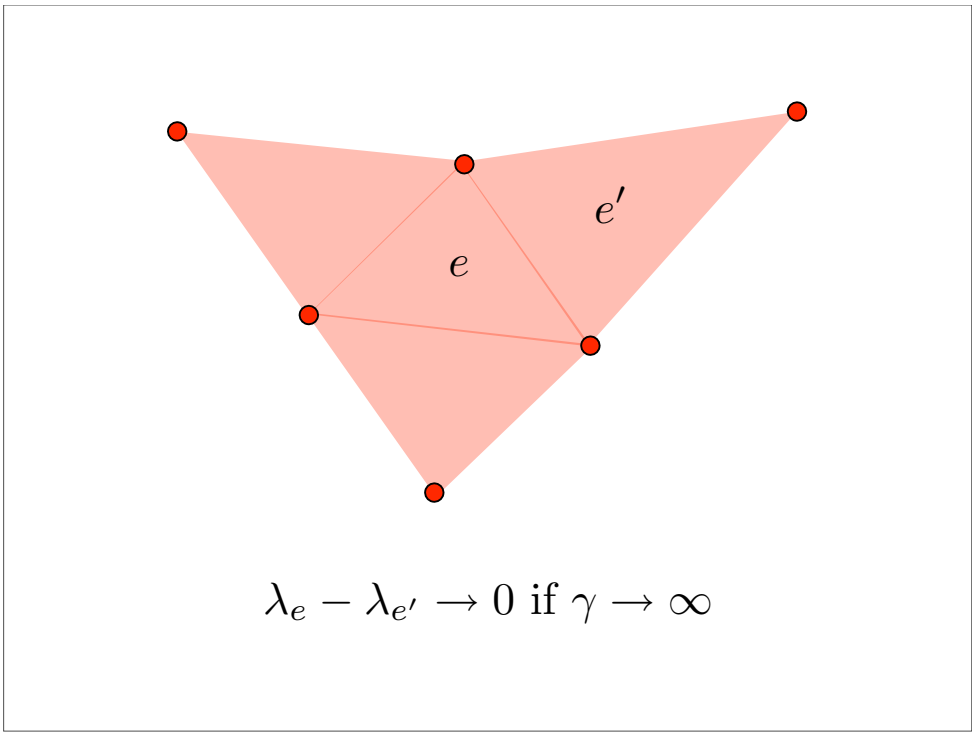

Figure 5.2: *An illustration of a spatial smoothness constraint equation.*

This constraint matrix allows us to write our final equation system as

$$\begin{bmatrix} \mathbf{S} & \mathbf{T} \\ \gamma_s^{\lambda}\mathbf{L}_s & \mathbf{O} \\ \mathbf{O} & \gamma_s^{\alpha}\mathbf{L}_s \end{bmatrix} \mathbf{p} = \begin{bmatrix} \bar{\mathbf{f}} \\ \mathbf{o} \\ \mathbf{o} \end{bmatrix} \tag{5.26}$$

from which we can get the parameter vector $\mathbf{p} = [\mathbf{l}|\mathbf{a}]^T$ by solving it in a least squares sense.

Note that two regularization parameters γ_s^{λ} and γ_s^{α} were used - one for each parameter type.

Fitting a Homogenous Isotropic Behavior

To get the over-dermined equation system that allows us to fit a homogenous isotropic behavior, we simply replace the λ_e's and α_e's in Equation 5.17 by the global constants λ and α and get:

$$\lambda \sum_e \mathbf{s}_e + \alpha \sum_e \mathbf{t}_e = [\mathbf{s}|\mathbf{t}] \begin{bmatrix} \lambda \\ \hline \alpha \end{bmatrix} = \mathbf{A}(\bar{\mathbf{x}})\mathbf{p} = \bar{\mathbf{f}} \tag{5.27}$$

where $\mathbf{s} = \sum_e \mathbf{s}_e$ and $\mathbf{t} = \sum_e \mathbf{t}_e$ are two long vectors and $\mathbf{A}(\bar{\mathbf{x}}) = [\mathbf{s}|\mathbf{t}]$ and $\mathbf{p} = [\lambda|\alpha]^T$ denote the new matrix and corresponding parameter vector, respectively.

Parameter Estimation Without Stiffness Warping

To get the equations for a fitting without stiffness warping, we can simply replace the rotation matrices $\mathbf{R}_e$ with 12×12 identity matrices $\mathbf{I}$.

The Equations 5.18 and 5.19 simplify to

$$\mathbf{s}_e = \mathbf{C}_e \left(\bar{\mathbf{x}} - \mathbf{x}_0 \right) = \mathbf{C}_e \bar{\mathbf{u}} \tag{5.28}$$

and

$$\mathbf{t}_e = \mathbf{D}_e \left(\bar{\mathbf{x}} - \mathbf{x}_0 \right) = \mathbf{D}_e \bar{\mathbf{u}} \tag{5.29}$$

if a measured displacement $\bar{\mathbf{u}}$ instead of a $\bar{\mathbf{x}}$ is used.

5.2.2 Simultaneous Analysis of Multiple Interactions

In this Subsection, the simultaneous force-based inverse analysis of a set of n interactions is discussed. We start with a short discussion on fitting a *single set* of material parameters to all of the n interactions. However, fitting a single set only allows to approximate a linear material behavior. More interesting is the simultaneous fitting of *multiple sets* - one per contact measurement. As we will see in Chapter 6, an interpolation between those fitted sets enables us to blend between the individual fitted FEM approximations during simulations of new interactions and thereby to approximate even non-linear interaction behavior. However, to make the interpolation of parameters feasible, the fitted properties not only have to be smooth within but also *across* fitted interactions. To this end, a second kind of smoothness is introduced that forces parameters of corresponding elements of different FEM approximates to be smooth.

In the following, we assume that a set of n acquired contact measurements is given

$$(\bar{\mathbf{x}}_i, \bar{\mathbf{f}}_i), i = 1, \ldots, n \tag{5.30}$$

and that a set of matrices

$$\mathbf{A}_i(\bar{\mathbf{x}}_i), i = 1, \ldots, n \tag{5.31}$$

are computed from them:

In case of inhomogeneous materials, those matrices are calculate by using the Equations 5.17, 5.18 and 5.19

$$[\mathbf{S}_i | \mathbf{T}_i], i = 1, \ldots, n \tag{5.32}$$

and in case of a homogeneous and isotropic materials by using 5.27:

$$[\mathbf{s}_i | \mathbf{t}_i], i = 1, \ldots, n \tag{5.33}$$

Fitting a Linear Inhomogeneous Material Behavior

A single set of inhomogeneous parameters $\mathbf{p} = [\mathbf{l}|\mathbf{a}]^T$ can be fitted to the n measured interactions by simply solving

$$\begin{bmatrix} \mathbf{S}_1 & \mathbf{T}_1 \\ \vdots & \vdots \\ \mathbf{S}_n & \mathbf{T}_n \\ \gamma_s^\lambda \mathbf{L}_s & \mathbf{O} \\ \mathbf{O} & \gamma_s^\alpha \mathbf{L}_s \end{bmatrix} \mathbf{p} = \begin{bmatrix} \bar{\mathbf{f}}_1 \\ \vdots \\ \bar{\mathbf{f}}_n \\ \mathbf{o} \\ \mathbf{o} \end{bmatrix} \tag{5.34}$$

in a least squares sense.

Furthermore, the corresponding weighted residual formulation is given as:

$$\hat{\mathbf{p}} = \arg\min_{\mathbf{p}} \left\{ \sum_{i=1}^{n} \left|\left|[\mathbf{S}_i|\mathbf{T}_i]\mathbf{p} - \bar{\mathbf{f}}_\mathbf{i}\right|\right|_2^2 + \left|\left|\mathbf{L}(\gamma_s^\lambda, \gamma_s^\alpha)\mathbf{p}\right|\right|_2^2 \right\} \tag{5.35}$$

with parameter vector $\mathbf{p} = [\mathbf{l}|\mathbf{a}]^T$ and constraint matrix

$$\mathbf{L}(\gamma_s^\lambda, \gamma_s^\alpha) = \begin{bmatrix} \gamma_s^\lambda \mathbf{L}_s & \mathbf{O} \\ \mathbf{O} & \gamma_s^\alpha \mathbf{L}_s \end{bmatrix} \tag{5.36}$$

Fitting a Linear Homogeneous Isotropic Material Behavior

In case of a single set of homogeneous and isotropic parameters $\mathbf{p} = [\lambda|\alpha]^T$, smoothness constraints are unnecessary and we get the over-determined equation system

$$\begin{bmatrix} \mathbf{s}_1 & \mathbf{t}_1 \\ \vdots & \vdots \\ \mathbf{s}_n & \mathbf{t}_n \end{bmatrix} \mathbf{p} = \begin{bmatrix} \bar{\mathbf{f}}_1 \\ \vdots \\ \bar{\mathbf{f}}_n \end{bmatrix} \tag{5.37}$$

that has to be solved in a least squares sense.

The corresponding residual formulation is unweighted and can be expressed as

$$\hat{\mathbf{p}} = \arg\min_{\mathbf{p}} \left\{ \sum_{i=1}^{n} \left|\left|[\mathbf{s}_i|\mathbf{t}_i]\mathbf{p} - \bar{\mathbf{f}}_\mathbf{i}\right|\right|_2^2 \right\} \tag{5.38}$$

where $\mathbf{p} = [\lambda|\alpha]^T$ denotes the parameter vector.

Fitting a Non-Linear Inhomogeneous Behavior

Let us now start with the discussion on the simultaneous fitting of *multiple sets* of parameters. We first observe that the n parameter vectors $\mathbf{p}_i = [\mathbf{l}_i|\mathbf{a}_i]^T$ can be fitted by sequentially solving

the independent equation systems (compare with Equation 5.26)

$$\begin{bmatrix} \mathbf{S}_i & \mathbf{T}_i \\ \gamma_s^\lambda \mathbf{L}_s & \mathbf{O} \\ \mathbf{O} & \gamma_s^\alpha \mathbf{L}_s \end{bmatrix} \mathbf{p}_i = \begin{bmatrix} \bar{\mathbf{f}}_i \\ \mathbf{o} \\ \mathbf{o} \end{bmatrix} \tag{5.39}$$

in a least squares sense.

By incorporating these independent systems into one bigger system, we can turn this sequential estimation procedure into a simultaneous one:

To this end, we collect all the matrices $\mathbf{S}_i$ and $\mathbf{T}_i$ in block diagonal matrices

$$\mathbf{S}^* = \operatorname{diag}(\mathbf{S}_1, \ldots, \mathbf{S}_n) \tag{5.40}$$

and

$$\mathbf{T}^* = \operatorname{diag}(\mathbf{T}_1, \ldots, \mathbf{T}_n) \tag{5.41}$$

Furthermore, a block diagonal matrix with n copies of the constraint matrix $\mathbf{L}_s$ is introduced

$$\mathbf{L}_s^* = \operatorname{diag}(\mathbf{L}_s, \ldots, \mathbf{L}_s) \tag{5.42}$$

If we now collect all the measured contact forces $\bar{\mathbf{f}}_i$ and all the $\mathbf{l}_i$'s and $\mathbf{a}_i$'s in vectors

$$\mathbf{f}^* = \left[\bar{\mathbf{f}}_1^T, \ldots, \bar{\mathbf{f}}_n^T\right]^T, \tag{5.43}$$

$$\mathbf{l}^* = [\mathbf{l}_1, \ldots, \mathbf{l}_n] \tag{5.44}$$

and

$$\mathbf{a}^* = [\mathbf{a}_1, \ldots, \mathbf{a}_n], \tag{5.45}$$

respectively, the equation system

$$\begin{bmatrix} \mathbf{S}^* & \mathbf{T}^* \\ \gamma_s^\lambda \mathbf{L}_s^* & \mathbf{O} \\ \mathbf{O} & \gamma_s^\alpha \mathbf{L}_s^* \end{bmatrix} \mathbf{p} = \begin{bmatrix} \mathbf{f}^* \\ \mathbf{o} \\ \mathbf{o} \end{bmatrix} \tag{5.46}$$

can be constructed, which enables us to simultaneously fit all n parameter sets by solving it for the unknown parameter vector $\mathbf{p} = \left[\mathbf{l}^* | \mathbf{a}^*\right]^T$.

However, as above-mentioned, further constraint equations have to be incorporated to not only enforce smoothness within, but also across the fitted parameter sets. To this end, a second constraint matrix $\mathbf{L}_m^*$ is introduced in the following:

As noted before, constraint equations are only dependent on geometry and not on the type of parameters. We therefore focus again on the λ's but our results equally hold for the parameters of the α-type.

Let us consider the two parameter vectors $\mathbf{l}_i$ and $\mathbf{l}_{i+1}$ of two different FEM approximations i and $i+1$, in which the parameters λ_e^i and λ_e^{i+1} of element e are highlighted:

$$\mathbf{l}_i = [\dots, \lambda_e^i, \dots] \tag{5.47}$$

and

$$\mathbf{l}_{i+1} = [\dots, \lambda_e^{i+1}, \dots] \tag{5.48}$$

Our goal is now to construct a set of constraint equations so that the differences between the parameters corresponding to the same element e, namely $\lambda_e^i - \lambda_e^{i+1}$, goes to zero if the regularization parameter goes to infinity (see Figure 5.3 for an illustration). This can be achieved by multiplying the vector $[\mathbf{l}_i, \mathbf{l}_{i+1}]^T$ by a block matrix $[\mathbf{I} - \mathbf{I}]$ (where $\mathbf{I}$ denotes the identity matrix), and setting it to zero. If we extend this observation to the set of all $\mathbf{l}$ vectors, we get our final constraint matrix

$$\mathbf{L}_m^* = \begin{bmatrix} \mathbf{I} & -\mathbf{I} & & & & \\ & \mathbf{I} & -\mathbf{I} & & & \\ & & \mathbf{I} & \ddots & & \\ & & & \ddots & -\mathbf{I} & \\ & & & & \mathbf{I} & -\mathbf{I} \end{bmatrix} \tag{5.49}$$

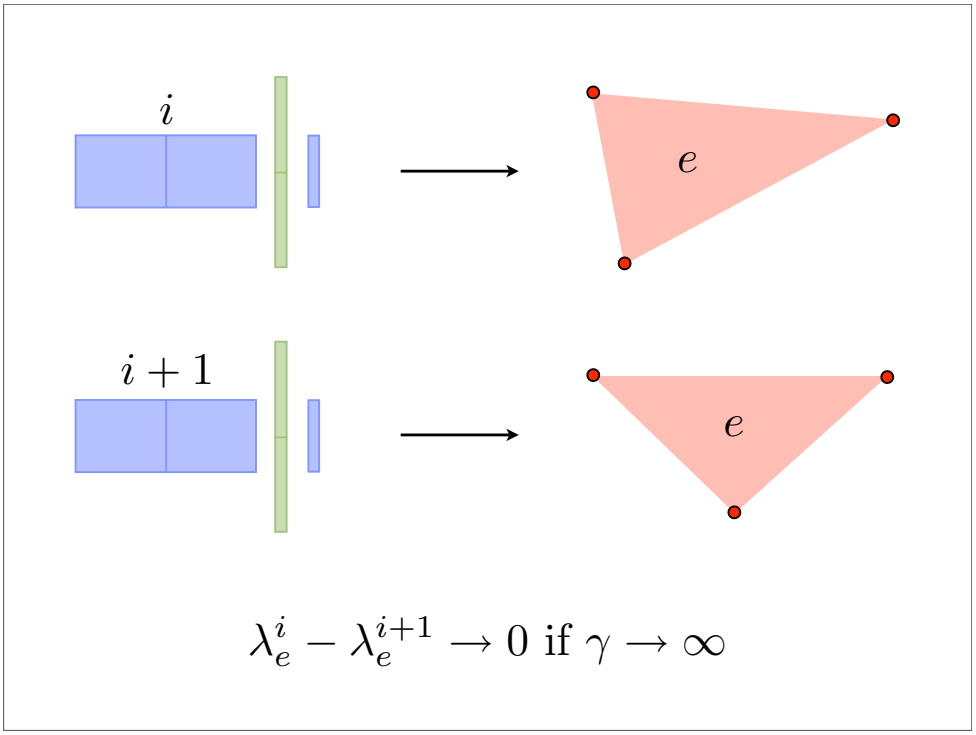

Figure 5.3: *An illustration of a smoothness constraint over two measurements i and $i+1$.*

If we now add this second kind of smoothness constraints to the system 5.46, we get our final

equation system

$$\begin{bmatrix} \mathbf{S}^* & \mathbf{T}^* \\ \gamma_s^\lambda \mathbf{L}_s^* & \mathbf{O} \\ \mathbf{O} & \gamma_s^\alpha \mathbf{L}_s^* \\ \gamma_m^\lambda \mathbf{L}_m^* & \mathbf{O} \\ \mathbf{O} & \gamma_m^\alpha \mathbf{L}_m^* \end{bmatrix} \mathbf{p} = \begin{bmatrix} \mathbf{f}^* \\ \mathbf{o} \\ \mathbf{o} \\ \mathbf{o} \\ \mathbf{o} \end{bmatrix} \tag{5.50}$$

that has to be solved in a least squares sense. Note that a set of four regularization parameters is used: Two to control the spatial smoothness of the individual parameter types and two to control their smoothness over the fitted interactions.

The corresponding weighted residual formulation is given as:

$$\hat{\mathbf{p}} = \arg\min_{\mathbf{p}} \left\{ \sum_{i=1}^{n} \left|\left| [\mathbf{S}_i | \mathbf{T}_i] \mathbf{p}_i - \bar{\mathbf{f}}_\mathbf{i} \right|\right|_2^2 + \left|\left| \mathbf{L}(\gamma_s^\lambda, \gamma_s^\alpha, \gamma_m^\lambda, \gamma_m^\alpha) \mathbf{p} \right|\right|_2^2 \right\} \tag{5.51}$$

with parameter vector $\mathbf{p} = [\mathbf{l}^* | \mathbf{a}^*]^T$ and constraint equations

$$\mathbf{L}(\gamma_s^\lambda, \gamma_s^\alpha, \gamma_m^\lambda, \gamma_m^\alpha) = \begin{bmatrix} \gamma_s^\lambda \mathbf{L}_s^* & \mathbf{O} \\ \mathbf{O} & \gamma_s^\alpha \mathbf{L}_s^* \\ \gamma_m^\lambda \mathbf{L}_m^* & \mathbf{O} \\ \mathbf{O} & \gamma_m^\alpha \mathbf{L}_m^* \end{bmatrix} \tag{5.52}$$

Fitting a Non-Linear Homogenous Isotropic Behavior

In case of multiple sets of homogenous isotropic parameters $\mathbf{p_i} = [\lambda^i, \alpha^i]^T$, the block diagonal matrices 5.40 and 5.41 reduce to

$$\mathbf{s}^* = \mathrm{diag}\,(\mathbf{s}_1, \ldots, \mathbf{s}_n) \tag{5.53}$$

and

$$\mathbf{t}^* = \mathrm{diag}\,(\mathbf{t}_1, \ldots, \mathbf{t}_n) \tag{5.54}$$

and the parameter vectors 5.44 and 5.45 to

$$\mathbf{l}^* = [\lambda_1, \ldots, \lambda_n] \tag{5.55}$$

and

$$\mathbf{a}^* = [\alpha_1, \ldots, \alpha_n] \tag{5.56}$$

Furthermore, the spatial smoothness constraints get unnecessary and the identity matrices in

5.49 reduce to 1's:

$$\mathbf{L}_m^* = \begin{bmatrix} 1 & -1 & & & & \\ & 1 & -1 & & & \\ & & 1 & \ddots & & \\ & & & \ddots & -1 & \\ & & & & 1 & -1 \end{bmatrix} \tag{5.57}$$

The equation system for multiple sets of homogeneous and isotropic parameters is therefore given as

$$\begin{bmatrix} \mathbf{s}^* & \mathbf{t}^* \\ \gamma_m^\lambda \mathbf{L}_m^* & \mathbf{O} \\ \mathbf{O} & \gamma_m^\alpha \mathbf{L}_m^* \end{bmatrix} \mathbf{p} = \begin{bmatrix} \mathbf{f}^* \\ \mathbf{o} \\ \mathbf{o} \end{bmatrix} \tag{5.58}$$

and we get the material parameters $\mathbf{p} = [\mathbf{l}^*|\mathbf{a}^*]^T$ by solving it in a least squares sense.

The corresponding weighted residual formulation is

$$\hat{\mathbf{p}} = \arg\min_{\mathbf{p}} \left\{ \sum_{i=1}^{n} \left|\left|[\mathbf{s}_i|\mathbf{t}_i]\mathbf{p}_i - \bar{\mathbf{f}}_\mathbf{i}\right|\right|_2^2 + \left|\left|\mathbf{L}(\gamma_m^\lambda, \gamma_m^\alpha)\mathbf{p}\right|\right|_2^2 \right\} \tag{5.59}$$

with parameter vector $\mathbf{p} = [\mathbf{l}^*|\mathbf{a}^*]^T$ and constraint equations

$$\mathbf{L}(\gamma_m^\lambda, \gamma_m^\alpha) = \begin{bmatrix} \gamma_m^\lambda \mathbf{L}_m^* & \mathbf{O} \\ \mathbf{O} & \gamma_m^\alpha \mathbf{L}_m^* \end{bmatrix} \tag{5.60}$$

5.3 Displacement-Based Inverse Analysis

In this Section, we perform a *displacement-based* inverse analysis of our interactions. We start again by analyzing an individual interaction before the simultaneous fitting of multiple sets is discussed in Subsection 5.3.2. As opposed to the force-based inverse analysis, this displacement-based approach leads to a non-linear inverse formulation and is therefore computationally more expensive. However, as we will see in Chapter 7, this non-linear parameter estimation turns out to be more robust in presence of noise and small measurement errors, which is inherently the case when working with real-world data. It gives us better results than the linear formulation from the previous Section. Note that the derivation of the displacement-based analysis follows a similar pattern as the one in 5.2. We therefore keep our discussion short.

5.3.1 Inverse Analysis of an Individual Contact Interaction

If we assume that the initial geometry $\mathbf{x}_0$ and the material parameters $\mathbf{p} = [\mathbf{l}|\mathbf{a}]^T$ of a deformable object are known, the deformation response on a contact $\mathbf{f}$ can be computed by solving the

equation system

$$\mathbf{K}'(\mathbf{p})\mathbf{x} = \mathbf{f} + \mathbf{K}''(\mathbf{p})\mathbf{x_0} \tag{5.61}$$

with stiffness matrices

$$\mathbf{K}'(\mathbf{p}) = \sum_e \mathbf{R}_e \mathbf{K}_e(\mathbf{p}_e)\mathbf{R}_e^T \tag{5.62}$$

and

$$\mathbf{K}''(\mathbf{p}) = \sum_e \mathbf{R}_e \mathbf{K}_e(\mathbf{p}_e) \tag{5.63}$$

and element stiffnesses

$$\mathbf{K}_e(\mathbf{p}_e) = \mathbf{K}_e(\lambda_e, \alpha_e) = \lambda_e \mathbf{C}_e + \alpha_e \mathbf{D}_e \tag{5.64}$$

for the unknown $\mathbf{x}$.

If we now multiply both sides of the equation system 5.61 with the stiffness matrix $\mathbf{K}'(\mathbf{p})$, we see that the parameterized deformation response on a measured contact $\bar{\mathbf{f}}$ can be expressed as

$$\mathbf{x}(\mathbf{p}) = \mathbf{K}'(\mathbf{p})^{-1}\left(\bar{\mathbf{f}} + \mathbf{K}''(\mathbf{p})\mathbf{x_0}\right) \tag{5.65}$$

Note that the inverse of the stiffness matrix $\mathbf{K}'$ is in general not sparse anymore.

Our displacement-based inverse problem is therefore to find the material parameters $\mathbf{p}$ that minimize the difference between the parameterized and the measured deformation response - expressed in formulas as:

$$\hat{\mathbf{p}} = \arg\min_{\mathbf{p}} \left\{ ||\mathbf{x}(\mathbf{p}) - \bar{\mathbf{x}}||_2^2 \right\} \tag{5.66}$$

However, this non-linear system of equations is, as the careful reader might expect, under-determined. We therefore have to include the spatial smoothness constraints from our linear formulation (see Subsection 5.2.1) to get our final weighted residual formulation:

$$\hat{\mathbf{p}} = \arg\min_{\mathbf{p}} \left\{ ||\mathbf{x}(\mathbf{p}) - \bar{\mathbf{x}}||_2^2 + ||\mathbf{L}(\gamma_s^\lambda, \gamma_s^\alpha)\mathbf{p}||_2^2 \right\} \tag{5.67}$$

with the constraint matrix

$$\mathbf{L}(\gamma_s^\lambda, \gamma_s^\alpha) = \begin{bmatrix} \gamma_s^\lambda \mathbf{L}_s & \mathbf{O} \\ \mathbf{O} & \gamma_s^\alpha \mathbf{L}_s \end{bmatrix} \tag{5.68}$$

The corresponding vector-valued function G that has to be solved in a non-linear least squares sense is given as

$$G(\mathbf{p}) = \begin{bmatrix} \mathbf{x}(\mathbf{p}) - \bar{\mathbf{x}} \\ \mathbf{L}(\gamma_s^\lambda, \gamma_s^\alpha)\mathbf{p} \end{bmatrix} \tag{5.69}$$

and its Jacobian can be expressed as:

$$J_G(\mathbf{p}) = \begin{bmatrix} J(\mathbf{p}) \\ \mathbf{L}(\gamma_s^\lambda, \gamma_s^\alpha) \end{bmatrix} \tag{5.70}$$

where $J(\mathbf{p})$ is the Jacobian of $\mathbf{x}(\mathbf{p}) - \bar{\mathbf{x}}$.

Note that the vector-valued function G is not convex in general. The optimization is therefore not guaranteed to converge to a global minima. However, we observe that the function is better behaved if a reasonably high regularization parameter is chosen.

The only missing part is the analytical expression for the Jacobian $J(\mathbf{p})$, whose derivation is given bellow.

The analytical expression for the element on the i-th row and the j-th column of $J(\mathbf{p})$ is given as:

$$\begin{aligned} J_{ij}(\mathbf{p}) &= \frac{\partial}{\partial p_j}\left[x_i(\mathbf{p}) - \bar{x}_i\right] \\ &= \frac{\partial}{\partial p_j}\left[\sum_k \mathbf{K'}^{-1}_{ik}(\mathbf{p}) f_k + \sum_k \sum_l \mathbf{K'}^{-1}_{ik}(\mathbf{p}) \mathbf{K''}_{kl}(\mathbf{p}) x_{0,l}\right] \\ &= \sum_k \left[\left[\frac{\partial}{\partial p_j}\mathbf{K'}^{-1}_{ik}(\mathbf{p})\right] f_k\right] + \sum_k \sum_l \left[\left[\frac{\partial}{\partial p_j}\mathbf{K'}^{-1}_{ik}(\mathbf{p})\right] \mathbf{K''}_{kl}(\mathbf{p}) x_{0,l}\right] \\ &+ \sum_k \sum_l \left[\mathbf{K'}^{-1}_{ik}(\mathbf{p}) \left[\frac{\partial}{\partial p_j}\mathbf{K''}_{kl}(\mathbf{p})\right] x_{0,l}\right] \end{aligned}$$

From this analytical expression of an individual element, we can derive the following expression for $J(\mathbf{p})$:

$$\begin{aligned} J(\mathbf{p}) &= \left[\ \cdots\ \middle|\ \tfrac{\partial \mathbf{K'}^{-1}}{\partial p_j}\bar{\mathbf{f}}\ \middle|\ \cdots\ \right] \\ &+ \left[\ \cdots\ \middle|\ \tfrac{\partial \mathbf{K'}^{-1}}{\partial p_j}\mathbf{K''}\mathbf{x}_0\ \middle|\ \cdots\ \right] \\ &+ \left[\ \cdots\ \middle|\ \mathbf{K'}^{-1}\tfrac{\partial \mathbf{K''}}{\partial p_j}\mathbf{x}_0\ \middle|\ \cdots\ \right] \end{aligned}$$

$$\frac{\partial \mathbf{K'}^{-1}}{\partial p_j} = -\mathbf{K'}^{-1}\frac{\partial \mathbf{K'}}{\partial p_j}\mathbf{K'}^{-1} \tag{5.71}$$

$$\frac{\partial \mathbf{K'}}{\partial p_j} = \begin{cases} \frac{\partial}{\partial \lambda_e}\mathbf{R}_e\left[\lambda_e\mathbf{C}_e + \alpha_e\mathbf{D}_e\right]\mathbf{R}_e^T = \left\{\mathbf{R}_e\mathbf{C}_e\mathbf{R}_e^T\right\} & \text{if } p_j = \lambda_e \\ \frac{\partial}{\partial \alpha_e}\mathbf{R}_e\left[\lambda_e\mathbf{C}_e + \alpha_e\mathbf{D}_e\right]\mathbf{R}_e^T = \left\{\mathbf{R}_e\mathbf{D}_e\mathbf{R}_e^T\right\} & \text{if } p_j = \alpha_e \end{cases} \tag{5.72}$$

$$\frac{\partial \mathbf{K''}}{\partial p_j} = \begin{cases} \frac{\partial}{\partial \lambda_e}\mathbf{R}_e\left[\lambda_e\mathbf{C}_e + \alpha_e\mathbf{D}_e\right] = \left\{\mathbf{R}_e\mathbf{C}_e\right\} & \text{if } p_j = \lambda_e \\ \frac{\partial}{\partial \alpha_e}\mathbf{R}_e\left[\lambda_e\mathbf{C}_e + \alpha_e\mathbf{D}_e\right] = \left\{\mathbf{R}_e\mathbf{D}_e\right\} & \text{if } p_j = \alpha_e \end{cases} \tag{5.73}$$

In the Equations 5.72 and 5.73, we used the notation $\{\mathbf{A}_e\}$ to indicate that the element matrix $\mathbf{A}_e$ is of global size.

Note that the above expression for $J(\mathbf{p})$ allows us to compute the Jacobian by only using one for-loop and matrix-vector multiplications otherwise. We also point out that the matrices in

5.72 and 5.73 are constant and also extremely sparse (only 16 3×3 blocks are non-zero). These constancy and sparsity properties enables pre-computation and also more efficient vector-matrix multiplications.

Fitting a Homogenous Isotropic Behavior

If we are only interested in fitting a homogeneous isotropic behavior, represented by a 2×1 parameter vector $\mathbf{p} = [\lambda, \alpha]^T$, the above expressions simplify tremendously:

The non-linear equation system in the residual formulation

$$\hat{\mathbf{p}} = \arg\min_{\mathbf{p}} \left\{ ||\mathbf{x}(\mathbf{p}) - \bar{\mathbf{x}}||_2^2 \right\} \tag{5.74}$$

is now overdetermined and regularization is therefore not needed.

The vector-valued function G simplifies to

$$G(\mathbf{p}) = \mathbf{x}(\mathbf{p}) - \bar{\mathbf{x}} \tag{5.75}$$

and its Jacobian is given as

$$\begin{aligned} J_G(\mathbf{p}) &= \left[\begin{array}{c|c} \frac{\partial \mathbf{K'}^{-1}}{\partial \lambda} \bar{\mathbf{f}} & \frac{\partial \mathbf{K'}^{-1}}{\partial \alpha} \bar{\mathbf{f}} \end{array} \right] \\ &+ \left[\begin{array}{c|c} \frac{\partial \mathbf{K'}^{-1}}{\partial \lambda} \mathbf{K''} \mathbf{x}_0 & \frac{\partial \mathbf{K'}^{-1}}{\partial \alpha} \mathbf{K''} \mathbf{x}_0 \end{array} \right] \\ &+ \left[\begin{array}{c|c} \mathbf{K'}^{-1} \frac{\partial \mathbf{K''}}{\partial \lambda} \mathbf{x}_0 & \mathbf{K'}^{-1} \frac{\partial \mathbf{K''}}{\partial \alpha} \mathbf{x}_0 \end{array} \right] \end{aligned}$$

with the matrices

$$\frac{\partial \mathbf{K'}}{\partial \lambda} = \frac{\partial}{\partial \lambda} \sum_e \mathbf{R}_e \left[\lambda \mathbf{C}_e + \alpha \mathbf{D}_e \right] \mathbf{R}_e^T = \sum_e \mathbf{R}_e \mathbf{C}_e \mathbf{R}_e^T \tag{5.76}$$

$$\frac{\partial \mathbf{K'}}{\partial \alpha} = \frac{\partial}{\partial \alpha} \sum_e \mathbf{R}_e \left[\lambda_e \mathbf{C}_e + \alpha_e \mathbf{D}_e \right] \mathbf{R}_e^T = \sum_e \mathbf{R}_e \mathbf{D}_e \mathbf{R}_e^T \tag{5.77}$$

$$\frac{\partial \mathbf{K''}}{\partial \lambda} = \frac{\partial}{\partial \lambda} \sum_e \mathbf{R}_e \left[\lambda \mathbf{C}_e + \alpha \mathbf{D}_e \right] = \sum_e \mathbf{R}_e \mathbf{C}_e \tag{5.78}$$

$$\frac{\partial \mathbf{K''}}{\partial \alpha} = \frac{\partial}{\partial \alpha} \sum_e \mathbf{R}_e \left[\lambda_e \mathbf{C}_e + \alpha_e \mathbf{D}_e \right] = \sum_e \mathbf{R}_e \mathbf{D}_e \tag{5.79}$$

5.3.2 Simultaneous Analysis of Multiple Interactions

In the following, we briefly discuss the simultaneous displacement-based inverse analysis of set of n interactions $(\bar{\mathbf{x}}_i, \bar{\mathbf{f}}_i), i = 1, \ldots, n$. However, because of the similarities to the force-based analysis, we only provide the weighted residual formulations here and leave it to the reader to derive the corresponding vector-valued functions G and their Jacobians J_G.

Fitting a Linear Inhomogeneous Behavior

In case of a single set of spatially varying parameters $\mathbf{p} = [\mathbf{l}|\mathbf{a}]^T$, the weighted residual formulation is given as

$$\hat{\mathbf{p}} = \arg\min_{\mathbf{p}} \left\{ \sum_{i=1}^{n} ||\mathbf{x}_i(\mathbf{p}) - \bar{\mathbf{x}}_i||_2^2 + ||\mathbf{L}(\gamma_s^\lambda, \gamma_s^\alpha)\mathbf{p}||_2^2 \right\} \tag{5.80}$$

with the constraint matrix

$$\mathbf{L}(\gamma_s^\lambda, \gamma_s^\alpha) = \begin{bmatrix} \gamma_s^\lambda \mathbf{L}_s & \mathbf{O} \\ \mathbf{O} & \gamma_s^\alpha \mathbf{L}_s \end{bmatrix} \tag{5.81}$$

Fitting a Linear Homogenous Isotropic Behavior

In case of a linear homogeneous isotropic behavior, the single set of globally constant parameters $\mathbf{p} = [\lambda|\alpha]^T$ can be found by minimizing the unweighted residual formulation

$$\hat{\mathbf{p}} = \arg\min_{\mathbf{p}} \left\{ \sum_{i=1}^{n} ||\mathbf{x}_i(\mathbf{p}) - \bar{\mathbf{x}}_i||_2^2 \right\} \tag{5.82}$$

in a least squares sense.

Fitting a Non-Linear Inhomogeneous Behavior

The multiple sets of spatially varying parameters $\mathbf{p}_i = [\mathbf{l}_i|\mathbf{a}_i]^T$, collected in a vector $\mathbf{p} = [\mathbf{l}^*|\mathbf{a}^*]^T$ with

$$\mathbf{l}^* = [\mathbf{l}_1, \ldots, \mathbf{l}_n] \tag{5.83}$$

and

$$\mathbf{a}^* = [\mathbf{a}_1, \ldots, \mathbf{a}_n], \tag{5.84}$$

can be estimated by using the following weighted residual formulation:

$$\hat{\mathbf{p}} = \arg\min_{\mathbf{p}} \left\{ \sum_{i=1}^{n} ||\mathbf{x}_i(\mathbf{p}_i) - \bar{\mathbf{x}}_i||_2^2 + ||\mathbf{L}(\gamma_s^\lambda, \gamma_s^\alpha, \gamma_m^\lambda, \gamma_m^\alpha)\mathbf{p}||_2^2 \right\} \tag{5.85}$$

with the constraints matrix

$$\mathbf{L}(\gamma_s^\lambda, \gamma_s^\alpha, \gamma_m^\lambda, \gamma_m^\alpha) = \begin{bmatrix} \gamma_s^\lambda \mathbf{L}_s^* & \mathbf{O} \\ \mathbf{O} & \gamma_s^\alpha \mathbf{L}_s^* \\ \gamma_m^\lambda \mathbf{L}_m^* & \mathbf{O} \\ \mathbf{O} & \gamma_m^\alpha \mathbf{L}_m^* \end{bmatrix} \tag{5.86}$$

where the block matrix $\mathbf{L}_m^*$ is defined as

$$\mathbf{L}_m^* = \begin{bmatrix} \mathbf{I} & -\mathbf{I} & & & & \\ & \mathbf{I} & -\mathbf{I} & & & \\ & & \mathbf{I} & \ddots & & \\ & & & \ddots & -\mathbf{I} & \\ & & & & \mathbf{I} & -\mathbf{I} \end{bmatrix} \tag{5.87}$$

Fitting a Non-Linear Homogeneous Isotropic Behavior

Last but not least, the estimation of multiple sets of homogenous isotropic parameters $\mathbf{p}_i = [\lambda_i|\alpha_i]^T$, collected in a vector $\mathbf{p} = [\mathbf{l}^*|\mathbf{a}^*]^T$ with

$$\mathbf{l}^* = [\lambda_1, \ldots, \lambda_n] \tag{5.88}$$

and

$$\mathbf{a}^* = [\alpha_1, \ldots, \alpha_n], \tag{5.89}$$

can be done by minimizing the weighted residual formulation

$$\hat{\mathbf{p}} = \arg\min_{\mathbf{p}} \left\{ \sum_{i=1}^{n} ||\mathbf{x}_i(\mathbf{p}_i) - \bar{\mathbf{x}}_i||_2^2 + ||\mathbf{L}(\gamma_m^\lambda, \gamma_m^\alpha)\mathbf{p}||_2^2 \right\} \tag{5.90}$$

with the constraint matrix

$$\mathbf{L}(\gamma_m^\lambda, \gamma_m^\alpha) = \begin{bmatrix} \gamma_m^\lambda \mathbf{L}_m^* & \mathbf{O} \\ \mathbf{O} & \gamma_m^\alpha \mathbf{L}_m^* \end{bmatrix} \tag{5.91}$$

and reduced block matrix

$$\mathbf{L}_m^* = \begin{bmatrix} 1 & -1 & & & & \\ & 1 & -1 & & & \\ & & 1 & \ddots & & \\ & & & \ddots & -1 & \\ & & & & 1 & -1 \end{bmatrix} \tag{5.92}$$

in a least squares sense.

6

Synthesis of New Interactions

In this Chapter, we discuss the primary motivation of our measurement-based approach, namely the synthesis of physically-plausible deformation behavior. In the last Chapter, we used inverse analysis to fit static linear FEM approximations to acquired measurements by identifying a set of model parameters. This parameter identification was performed for a collection of different material behaviors including linear and non-linear, homogenous isotropic and also inhomogeneous ones. Hence, all the requisites for an accurate direct analysis are met and deformations on new contacts can be computed. However, simulations of contact interactions are dynamic and our analysis and acquisition of interactions was exclusively performed for the static case. We therefore use force or load instead of time increments in our synthesis.

We also integrated stiffness warping [Müller and Gross 2004] in our simulation loop. Note that stiffness warping, as discussed in [Müller and Gross 2004], assumes a dynamic FEM simulation. In contrast to their work, stiffness warping is used in a static context here. These warped stiffnesses together with the incremental loading enables us to effectively approximate geometric non-linearities which would lead otherwise to severe artifacts under large deformations due to the linear Cauchy strain tensor.

For non-linear material behavior, however, the model has to be further extended. This non-linear behavior is modeled by smoothly changing material parameter sets by an interpolation in the corresponding parameter space. We use two different schemes in our simulation framework: For homogeneous non-linear materials, a simple RBF-based interpolation scheme [Carr et al. 2001] is adopted, and, for an inhomogeneous material behavior, we employ a novel strain-based interpolation technique similar to [Bickel et al. 2007]. The interpolation of estimated parameters using these two schemes allows us to *blend* the corresponding fitted linear FEM approximations during the synthesis phase and thereby to approximate non-linear stress-strain relations. Furthermore, the additional computational cost for the interpolation of parameters in our simulation loop is low and allows synthesis of non-linear interaction behavior at interactive rates.

This Chapter is organized as follows: In the next Section, we briefly introduce the concept of incremental loading and also discuss the integration of warped stiffnesses into our simulation loop. The resulting synthesis is then further refined in Section 6.2 to synthesize contacts with different kinds of material behaviors. We discuss our two interpolation schemes in Subsections 6.2.3 and 6.2.4.

6.1 Incremental Loading and Stiffness Warping

Let us assume that an object with initial geometry $\mathbf{x}_0$ and unspecified linear stress-strain relation is given. To simulate the dynamic behavior of this object upon a contact $\mathbf{f}$, the vector $\mathbf{x}$ is usually made time-dependent and a discretized version of the following ordinary differential equation (ODE) of second order is used:

$$\mathbf{M}\ddot{\mathbf{x}} + \mathbf{C}\dot{\mathbf{x}} + \mathbf{K}(\mathbf{x} - \mathbf{x}_0) = \mathbf{f} \tag{6.1}$$

where $\mathbf{M}$ denotes the mass, $\mathbf{C}$ the damping and $\mathbf{K}$ the stiffness matrix.

In our framework, however, a discretization based on time increments, even though possible, is not in the line with our static analysis and acquisition. The fundamental observation on which our approach is based on is that accurate direct analysis can only be made if inverse analysis was solved to determine the model parameters. However, our acquisition system is only acquiring the static deformation behavior of an object. Furthermore, an object's density distribution – required to construct a physically-accurate mass matrix $\mathbf{M}$ – is not measured. We therefore use load instead of time increments to synthesize our interactions. To this end, the force vector $\mathbf{f}$ is split into increments of length Δf as illustrated in Figure 6.1.

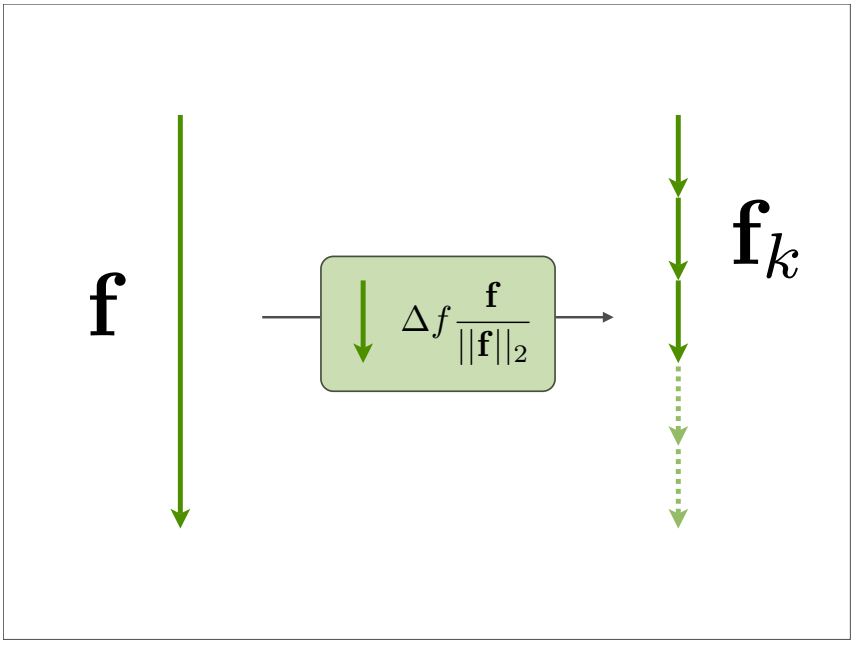

Figure 6.1: *Illustration of the incremental loading.*

The simulation loop based on our static direct analysis (compare with Equations 3.64, 3.65 and 3.66) together with the incremental loading can be summarized as:

precomputations
  forall elements e compute $\mathbf{K}_e$
end precomputations
initialization
  $\mathbf{x}_k := \mathbf{x}_0$
  $\mathbf{f}_k := \mathbf{o}$
end initialization
loop
  if $||\mathbf{f}_k||_2 + \Delta f < ||\mathbf{f}||_2$ **then**
    $\mathbf{f}_{k+1} := \mathbf{f}_k + \Delta f \frac{\mathbf{f}}{||\mathbf{f}||_2}$
  else
    break
  end if
  forall elements e compute $\mathbf{R}_e$ from $\mathbf{x}_{0e}$ to $\mathbf{x}_{k,e}$
  assemble $\mathbf{K}' = \sum_e \mathbf{R}_e \mathbf{K}_e \mathbf{R}_e^T$
  assemble $\mathbf{K}'' = \sum_e \mathbf{R}_e \mathbf{K}_e$
  solve $\mathbf{K}'\mathbf{x}_{k+1} = \mathbf{f}_{k+1} + \mathbf{K}''\mathbf{x}_0$ for $\mathbf{x}_{k+1}$
  $\mathbf{x}_k := \mathbf{x}_{k+1}$
  $\mathbf{f}_k := \mathbf{f}_{k+1}$
end loop

Note that we use warped stiffnesses in the above loop.

This simulation loop is refined in the following Section so that contacts with objects of specific material behaviors can be synthesized.

6.2 Simulation of Deformations Using Various Material Models

In Chapter 5, we used inverse analysis to estimate a set of material parameters. We use those fitted parameters here to synthesize physically-plausible interactions upon new contacts $\mathbf{f}$. In case of a linear material, we only have one set of parameters that describes the deformation behavior through the whole simulation. The synthesis of contacts with linear homogeneous and inhomogeneous materials is discussed in the next two Subsections. More interesting are the cases, in which interpolation and multiple parameter sets are involved, namely the cases where non-linear behavior is approximated. The synthesis of the non-linear behaviors with their corresponding interpolation schemes are discussed in the Subsections 6.2.3 and 6.2.4.

6.2.1 Linear Homogeneous Isotropic Material

In case of an object with a linear homogeneous isotropic material behavior, only two global elasticity constants, namely λ and α, are fitted. Those constants do not change during the synthesis and the element stiffnesses can therefore be pre-computed as follows:

precomputations
forall elements e compute $\mathbf{C}_e$ and $\mathbf{D}_e$
forall elements e compute $\mathbf{K}_e = \lambda \mathbf{C}_e + \alpha \mathbf{D}_e$
end precomputations

The rest of the simulation loop stays the same.

6.2.2 Linear Inhomogeneous Material

We model linear inhomogeneous materials by fitting a single set of spatially varying parameters λ_e and α_e. Those parameters, as the linear homogeneous ones, do not change during simulations of new contacts and the element stiffnesses can be pre-computed by using Equation 3.63:

precomputations
forall elements e compute $\mathbf{C}_e$ and $\mathbf{D}_e$
forall elements e compute $\mathbf{K}_e = \lambda_e \mathbf{C}_e + \alpha_e \mathbf{D}_e$
end precomputations

The synthesis loop is unchanged otherwise.

6.2.3 Non-Linear Homogeneous Isotropic Material

If an object of initial geometry $\mathbf{x}_0$ and with non-linear homogeneous isotropic material behavior is given, multiple parameter sets (λ^i, α^i) are fitted to the individual measured deformation responses $(\bar{\mathbf{x}}_i, \bar{\mathbf{f}}_i)$. Because we have now deformation-dependent parameters, interpolation has to be used in our synthesis loop. This interpolation in parameter space allows us to effectively approximate a non-linear stress-strain-relation of a homogeneous isotropic material. For the interpolation, we employ Radial Basis Functions (RBF's) [Carr et al. 2001]. During the simulation loop, the current deformation response $\mathbf{x}_k$ is used to calculate the new parameter values by using the following weighted sums:

$$\lambda = \sum_i w_i^\lambda \phi(||\mathbf{x}_k - \bar{\mathbf{x}}_i||_2) \tag{6.2}$$

$$\alpha = \sum_i w_i^\alpha \phi(||\mathbf{x}_k - \bar{\mathbf{x}}_i||_2) \tag{6.3}$$

We use the Euclidean distance metric to compute the differences between the current and measured deformation responses and employ biharmonic basis functions in our current implementation.

The RBF weights $\mathbf{w}^\lambda = [\ldots, w_i^\lambda, \ldots]^T$ and $\mathbf{w}^\alpha = [\ldots, w_i^\alpha, \ldots]^T$ can be pre-computed by solving two systems of equations

$$\Phi \mathbf{w}^\lambda = [\ldots, \lambda^i, \ldots]^T \tag{6.4}$$

and

$$\Phi \mathbf{w}^\alpha = [\ldots, \alpha^i, \ldots]^T \tag{6.5}$$

where the matrix Φ is defined as $\Phi_{ij} = \phi(||\bar{\mathbf{x}}_i - \bar{\mathbf{x}}_j||)$.

The synthesis loop can therefore be summarized as:

precomputations
  forall elements e compute $\mathbf{C}_e$ and $\mathbf{D}_e$
  forall measurements i compute weights w_i^λ and w_i^α
end precomputations
initialization
  $\mathbf{x}_k := \mathbf{x}_0$
  $\mathbf{f}_k := \mathbf{o}$
end initialization
loop
  if $||\mathbf{f}_k||_2 + \Delta f < ||\mathbf{f}||_2$ **then**
    $\mathbf{f}_{k+1} := \mathbf{f}_k + \Delta f \frac{\mathbf{f}}{||\mathbf{f}||_2}$
  else
    break
  end if
  forall elements e compute $\mathbf{R}_e$ from $\mathbf{x}_{0e}$ to $\mathbf{x}_{k,e}$
  interpolate $\lambda = \sum_i w_i^\lambda \phi(||\mathbf{x}_k - \bar{\mathbf{x}}_i||_2)$
  interpolate $\alpha = \sum_i w_i^\alpha \phi(||\mathbf{x}_k - \bar{\mathbf{x}}_i||_2)$
  forall elements e compute $\mathbf{K}_e = \lambda \mathbf{C}_e + \alpha \mathbf{D}_e$
  assemble $\mathbf{K}' = \sum_e \mathbf{R}_e \mathbf{K}_e \mathbf{R}_e^T$
  assemble $\mathbf{K}'' = \sum_e \mathbf{R}_e \mathbf{K}_e$
  solve $\mathbf{K}' \mathbf{x}_{k+1} = \mathbf{f}_{k+1} + \mathbf{K}'' \mathbf{x}_0$ for $\mathbf{x}_{k+1}$
  $\mathbf{x}_k := \mathbf{x}_{k+1}$
  $\mathbf{f}_k := \mathbf{f}_{k+1}$
end loop

Note that the element stiffnesses are now changing depending on the actual deformed state of the object.

6.2.4 Non-Linear Inhomogeneous Material

As we discussed in Sections 5.2 and 5.3, a non-linear inhomogeneous material is approximated by fitting multiple sets of spatially varying parameters

$$\mathbf{p}_i = [\mathbf{l}_i | \mathbf{a}_i]^T \tag{6.6}$$

with $\mathbf{l}_i = [\ldots, \lambda_e^i, \ldots]$ and $\mathbf{a}_i = [\ldots, \alpha_e^i, \ldots]$ to the individual measurements $(\bar{\mathbf{x}}_i, \bar{\mathbf{f}}_i)$.

We propose a novel strain-based interpolation technique similar to [Bickel et al. 2007] to interpolate between estimated parameters in parameter space:

The element strain ε_e, as defined in Equation 3.49, provides a powerful measurement of an element's change in form and size. It therefore seems to be natural to incorporate those ε_e's in an interpolation scheme used to interpolate element parameters over space and measurements. To this end, we collect all the fitted element strains $\bar{\varepsilon}_e^i$ (6×1 vectors) of measurement i in vectors:

$$\bar{\mathbf{e}}_i = [\ldots, (\bar{\varepsilon}_e^i)^T, \ldots]^T \tag{6.7}$$

The fitted element strain $\bar{\varepsilon}_e^i$ corresponding to element e and measurement i can be computed by using

$$\bar{\varepsilon}_e^i = \mathbf{B}_e (\bar{\mathbf{R}}_e^i)^T (\bar{\mathbf{x}}_{i,e} - \mathbf{x}_{0e}) \tag{6.8}$$

where the matrices $\bar{\mathbf{R}}_e^i$ denote the fitted rotations.

During simulations, the current deformation response $\mathbf{x}_k$ is used to compute the global strain vector $\mathbf{e}$, which in turn allows us to interpolate the element parameters λ_e and α_e by using the following weighted sums:

$$\lambda_e = \sum_l w_{e,l}^{\lambda} \phi(||\mathbf{e} - \bar{\mathbf{e}}_l||_e) \tag{6.9}$$

and

$$\alpha_e = \sum_l w_{e,l}^{\alpha} \phi(||\mathbf{e} - \bar{\mathbf{e}}_l||_e) \tag{6.10}$$

where we used a locally-weighted strain-based distance metric (compare with [Bickel et al. 2007])

$$||\mathbf{e} - \bar{\mathbf{e}}_l||_e = \sqrt{\sum_{e'} ||\varepsilon_{e'} - \bar{\varepsilon}_{e'}^i||_2^2 e^{-c||\varepsilon_{e'} - \bar{\varepsilon}_e^i||_2^2}} \tag{6.11}$$

Note that the parameter c can be used to control the degree of decay.

The weights $w_{e,l}^{\lambda}$ and $w_{e,l}^{\alpha}$ used in the above weighted sums, can be pre-computed by solving a set of element-wise equation systems:

1. Compute matrices $\Phi_{e,p,q} = \phi(||\bar{\mathbf{e}}_p - \bar{\mathbf{e}}_q||_e)$ for all elements e (p and q denote measurement indices).
2. Form the parameter vectors $\mathbf{b}_e^{\lambda} = [\ldots, \lambda_e^i, \ldots]$ and $\mathbf{b}_e^{\alpha} = [\ldots, \alpha_e^i, \ldots]$ for all elements e (i denotes the measurement index)
3. Compute the weight vectors $\mathbf{w}_e^{\lambda} = [\ldots, w_{e,i}^{\lambda}, \ldots]$ and $\mathbf{w}_e^{\alpha} = [\ldots, w_{e,i}^{\alpha}, \ldots]$ (i denotes the measurement index) by solving $\Phi_e \mathbf{w}_e^{\lambda} = \mathbf{b}_e^{\lambda}$ and $\Phi_e \mathbf{w}_e^{\alpha} = \mathbf{b}_e^{\alpha}$ for every element e.

The resulting synthesis loop can be summarized as:

precomputations
  forall elements e compute $\mathbf{C}_e$ and $\mathbf{D}_e$
  forall elements e and measurements i compute weights $w^{\lambda}_{e,i}$ and $w^{\alpha}_{e,i}$
end precomputations
initialization
  $\mathbf{x}_k := \mathbf{x}_0$
  $\mathbf{f}_k := \mathbf{o}$
end initialization
loop
  if $||\mathbf{f}_k||_2 + \Delta f < ||\mathbf{f}||_2$ **then**
    $\mathbf{f}_{k+1} := \mathbf{f}_k + \Delta f \frac{\mathbf{f}}{||\mathbf{f}||_2}$
  else
    break
  end if
  forall elements e compute $\mathbf{R}_e$ from $\mathbf{x}_{0e}$ to $\mathbf{x}_{k,e}$
  forall elements e compute strains $\varepsilon_e = \mathbf{B}_e \mathbf{R}_e^T (\mathbf{x}_{k,e} - \mathbf{x}_{0e})$
  construct $\mathbf{e}$ from strains ε_e
  forall elements e interpolate $\lambda_e = \sum_i w^{\lambda}_{e,i} \phi(||\mathbf{e} - \bar{\mathbf{e}}_i||_e)$
  forall elements e interpolate $\alpha_e = \sum_i w^{\alpha}_{e,i} \phi(||\mathbf{e} - \bar{\mathbf{e}}_i||_e)$
  forall elements e compute $\mathbf{K}_e = \lambda_e \mathbf{C}_e + \alpha_e \mathbf{D}_e$
  assemble $\mathbf{K}' = \sum_e \mathbf{R}_e \mathbf{K}_e \mathbf{R}_e^T$
  assemble $\mathbf{K}'' = \sum_e \mathbf{R}_e \mathbf{K}_e$
  solve $\mathbf{K}' \mathbf{x}_{k+1} = \mathbf{f}_{k+1} + \mathbf{K}'' \mathbf{x}_0$ for $\mathbf{x}_{k+1}$
  $\mathbf{x}_k := \mathbf{x}_{k+1}$
  $\mathbf{f}_k := \mathbf{f}_{k+1}$
end loop

7

Model Validation

Model validation is an important step in the model building sequence. In our case, a in-depth analysis would include a thorough investigation of both, our parameter estimation techniques and also of our synthesis with its corresponding interpolation schemes. In this Chapter, however, only our non-linear displacement-based estimation technique is investigated. We use a data set consisting of four individual force-displacement measurements of our sponge as a basis for our discussion (see Figure 7.1). The presented results show the influence of both kinds of smoothness constraints that are weighted with regularization parameters.

7.1 Fitting a Homogeneous Material Behavior

The result of fitting two homogenous and isotropic parameters to measurement 4 is illustrated in Figure 7.2. The color coding shows the fitting error: In the red areas, the fitting error is around 5 mm, yellow means an error of about 2 mm and grey indicates areas where the error is bellow 1 mm. The results of the independent fitting of two globally constant homogeneous and isotropic material parameters to the four measurements are summarized in Table 7.1. We observe that the Young's moduli E are always positive and seem to be in a physically-plausible range. The fitted Poisson ratio, however, is only positive for measurement 1 and is negative otherwise. As mentioned in Chapter 3, such a material behavior is rare.

The results of fitting two global isotropic elasticity constants to all 4 measurements are summarized in Table 7.2. We observe that the measurement 4 has the most influence on the fitted parameters.

We also fitted multiple sets of homogeneous isotropic parameters to the four measurements. The corresponding results are summarized in Table 7.3. We included weighted smoothness

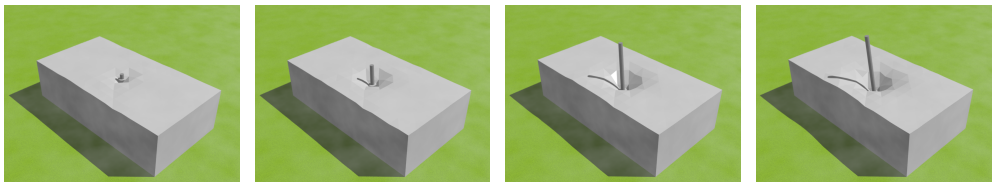

(1) (2) (3) (4)

Figure 7.1: *A set of 4 example deformations.*

measurement i	1	2	3	4
λ^i	1.1614	1.2730	1.1445	0.9347
α^i	0.0039	-0.0083	-0.2291	-0.2802
E^i	1.1574	1.2812	1.2819	1.0468
ν^i	0.0034	-0.0065	-0.2002	-0.2998
min. error [mm]	0.0043	0.0133	0.0592	0.0549
avg. error [mm]	0.0295	0.0829	0.1749	0.2334
max. error [mm]	0.2226	0.3716	0.6132	0.7012
res. norm [mm]	0.5576	1.3820	2.7450	3.5654

Table 7.1: *Fitting two homogeneous isotropic parameters to each measurement independently.*

constraints over the measurements in our optimization. We observe that a high regularization ($\gamma = 1000.0$) leads to the same results as in Table 7.2. On the other hand, if the regularization is relaxed ($\gamma = 0.01$), the results are very close to the ones we got for our individual fits (compare with values in Table 7.1.

7.2 Fitting a Inhomogeneous Material Behavior

The results of fitting a linear homogeneous material behavior to the measurement 4 of our data set is summarized in Figure 7.3 and the simultaneous fitting of a non-linear inhomogeneous material behavior to all four measurements is illustrated in Figures 7.4 and 7.5.

measurement i	1	2	3	4
λ	1.0237			
α	-0.2448			
E	1.1514			
ν	-0.2392			
min. error [mm]	0.0054	0.0141	0.0498	0.0713
avg. error [mm]	0.0302	0.0878	0.1801	0.2302
max. error [mm]	0.2845	0.3696	0.5603	0.7371
res. norm [mm]	4.7746			

Table 7.2: *Fitting a linear homogeneous isotropic material behavior to all 4 measurements.*

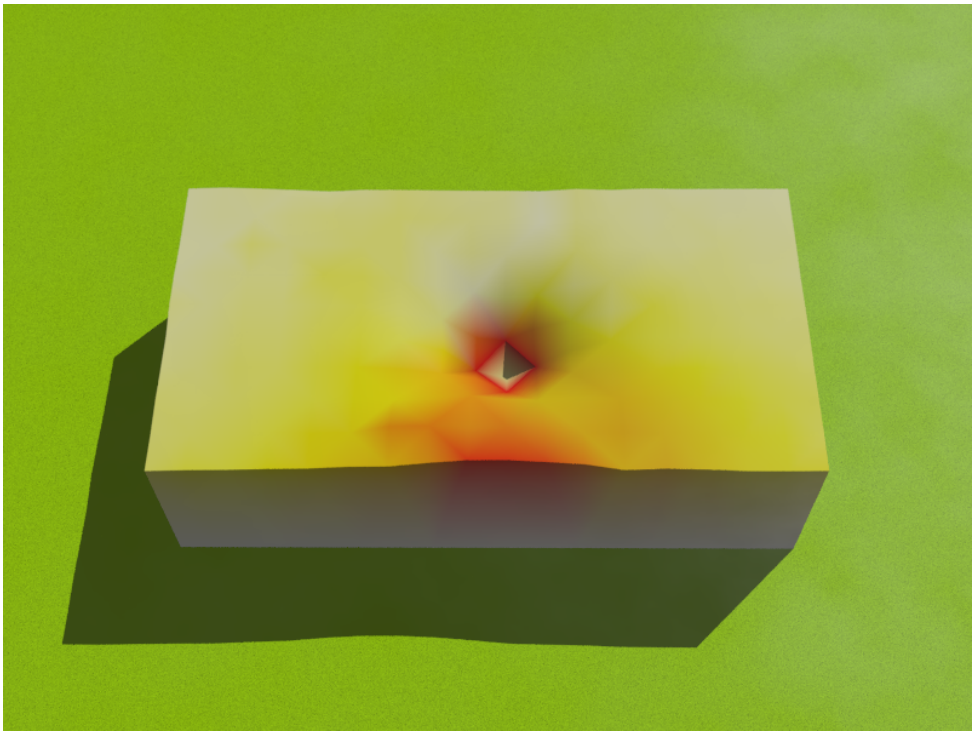

Figure 7.2: *Fitting a homogeneous isotropic material behavior to measurement 4.*

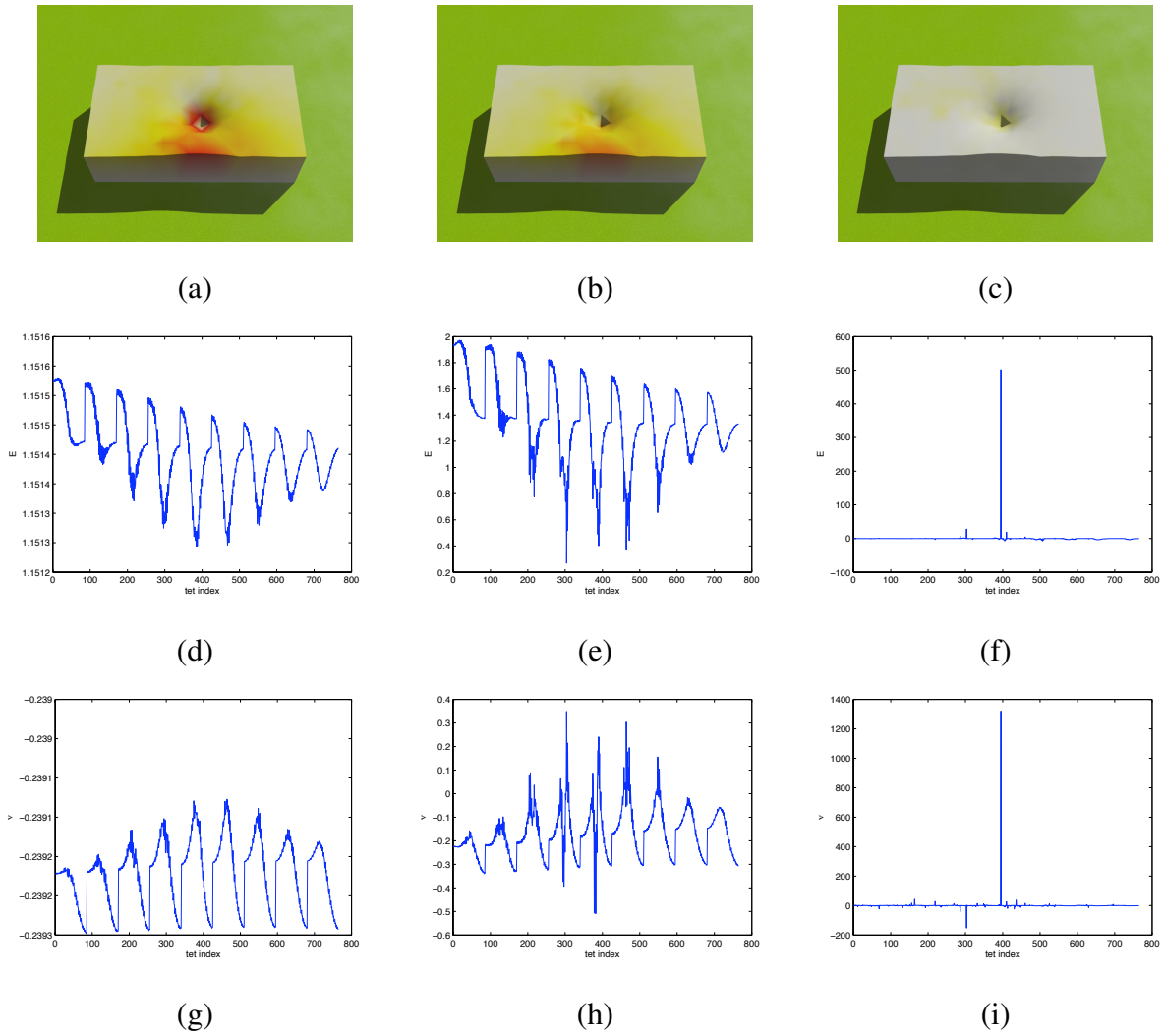

Figure 7.3: *Fitting a set of spatially varying parameters to measurement 4. We used spatial smoothness constraints controlled by a regularization parameter γ_s in our non-linear least squares formulation. Left column: $\gamma_s = 100.0$. Middle column: $\gamma_s = 1.0$. Right column: $\gamma_s = 0.1$. The images on the top row, namely (a), (b) and (c), show the color-coded fitting error. On the second row ((d), (e) and (f)) plots of the fitted Young's moduli are shown. The plots on the bottom row, namely (g), (h) and (i) show the fitted Poisson ratio's. We observe that the smoothness of parameters and the fitting error decrease from the left to the right column as someone would expect (see Figure 5.1). The results in the right column are clearly an over-fitting.*

measurement i		1	2	3	4
$\gamma_m^{\{\lambda,\alpha\}} = 0.01$	λ^i	1.1614	1.2730	1.1445	0.9347
	α^i	0.0038	-0.0083	-0.2291	-0.2802
	E^i	1.1576	1.2812	1.2819	1.0469
	ν^i	0.0033	-0.0065	-0.2002	-0.2998
$\gamma_m^{\{\lambda,\alpha\}} = 1000.0$	λ^i	1.0237	1.0237	1.0237	1.0237
	α^i	-0.2448	-0.2448	-0.2448	-0.2448
	E^i	1.1514	1.1514	1.1514	1.1514
	ν^i	-0.2392	-0.2392	-0.2392	-0.2392

Table 7.3: *Fitting a non-linear homogeneous isotropic material behavior to the 4 measurements.*

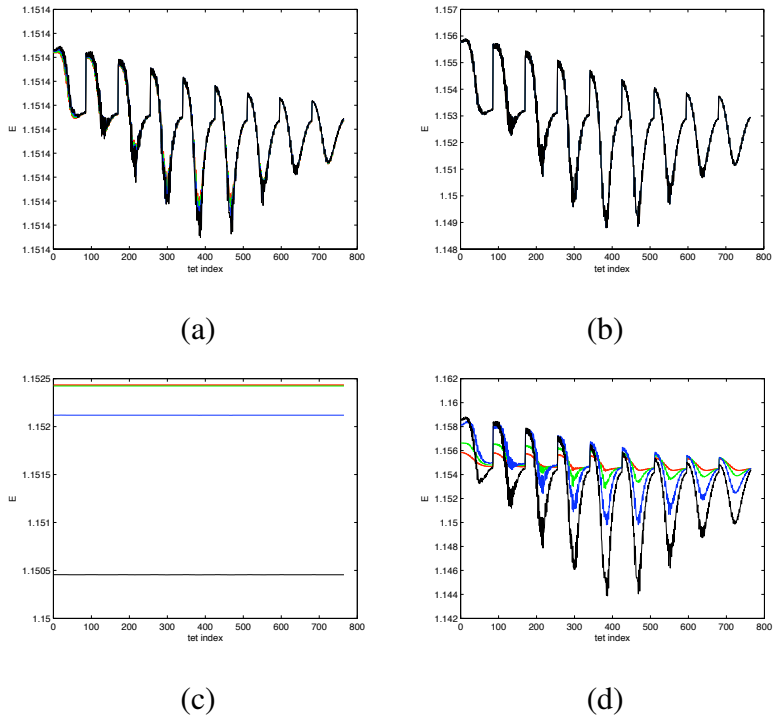

Figure 7.4: *Fitting multiple sets of spatially varying parameters by using constraints within (controlled by the regularization parameter γ_s) and across (controlled by the regularization parameter γ_m) the 4 measurements (1:red, 2:green, 3:blue, 4:black). The four plots show the fitted Young's moduli. The regularization parameters are set to (a) $\gamma_s = 1000$ and $\gamma_m = 1000$, (b) $\gamma_s = 10$ and $\gamma_m = 1000$, (c) $\gamma_s = 1000$ and $\gamma_m = 1$ and (d) $\gamma_s = 10$ and $\gamma_m = 1$. If the smoothness constraints over the measurements, controlled by γ_s, are relaxed (top row to bottom row), the parameters are less smooth over the individual measurements. On the other hand, if the spatial smoothness constraints are relaxed (from left column to right column) the range of parameter values increase and the resulting parameters are less smooth within the individual measurements.*

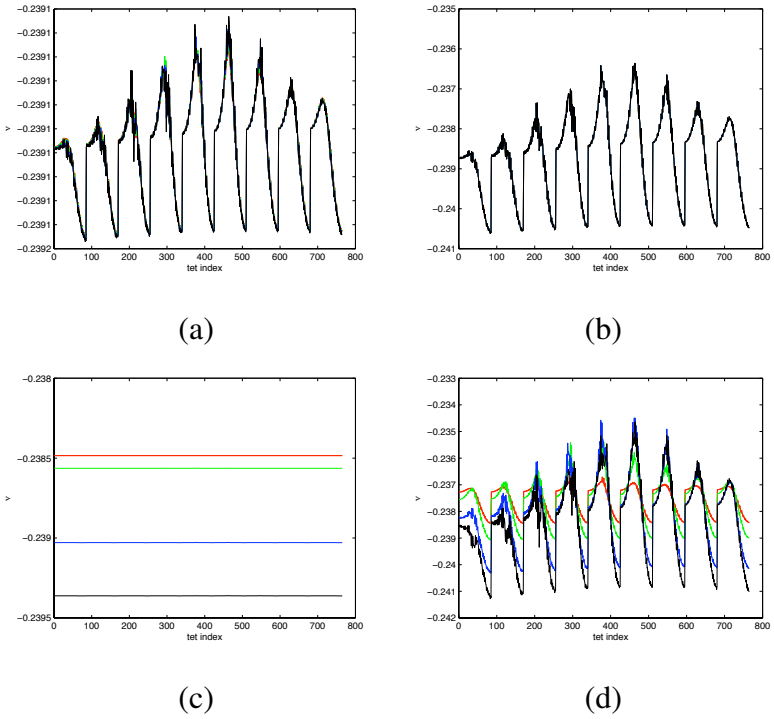

Figure 7.5: *Same experiment as in Figure 7.4, but the plots are showing the fitted Poisson ratios instead.*

8

Conclusion and Outlook

This thesis investigated non-linear deformation behavior of solid objects and presented a novel measurement-based deformation model. The model is based on FEM theory and allows to estimate material properties from a set of example data. During runtime, physically-plausible non-linear deformations can effectively and efficiently be simulated by interpolating material properties in a suitable material space.

We started by acquiring a comprehensive set of example deformations. By using force probes and a marker-based stereo-vision system, an object was sampled at several different locations with varying force intensities. The resulting force-displacement measurements were recorded and stored in a database.

We investigated deformation techniques based on FEM modeling to formulate an inverse problem that has material parameters as its unknowns. It turned out that the inverse problem, given only a small set of force-displacement measurements, is ill-posed. However, by using regularization techniques based on smoothness constraints between neighboring and corresponding elements within and across measurements, we were able to successfully turn our ill-posed displacement-based inverse formulation into a well-posed one.

In general, there are two possibilities to formulate the regularized inverse as a least squares problem: Either, the error of the displacement field, or the error of the force field is minimized.

Minimizing the error of the displacement field results in a non-linear least squares optimization, whereas the force-based approach can be stated as a linear least squares problem. The computationally more efficient minimization of the force error, however, turned out to be very sensitive to noise and also to be badly conditioned. On the other side, the non-linear optimization function based on the displacement error is not convex in general and therefore more challenging to fit. Another major drawback of the non-linear formulation is its computational cost caused by a inverse stiffness matrix that destroys the sparsity structure of the included matrices. We

observed, however, that reasonable regularization parameters together with physically-plausible initial start values lead to a well-behaved target function. The resulting fitting techniques can then be used to estimate material properties that range from linear homogeneous and isotropic to non-linear inhomogeneous behaviors.

Fitting material parameters of static linear-FEM approximations can basically be viewed as fitting deformation approximations. Our novel locally-weighted strain-based interpolation scheme used to interpolate estimated parameters in parameter space can therefore be viewed as a blending of linear approximations. Interpolation and fitting together allows to synthesize new non-linear interactions, even though computationally efficient and numerically stable *linear* deformable FEM is used. Concluding, our measurement-based approach therefore fills the gap between linear deformable FEM models and their non-linear formulations.

However, there are still several open question and potential improvements. Our interpolations are based on RBF's which are known to extrapolate badly. The extrapolation behavior has therefore to be further investigated. We also need to run more validation on our model when new deformations are synthesized. That includes leave-one out and also cross-validations.

Interesting future work would be to extend our FEM-based model to also include the dynamic behavior of deformable objects. Our inverse formulation and also our data acquisition would have to be extended to estimate and measure, for instance, and object's density distribution.

We believe that our pioneering and interdisciplinary work has great potential to be useful in the development of more accurate physically-based deformable models in computer graphics. Future applications could include a data-base of measured deformation behaviors that allow a special-effect animator to add different kinds of material behavior to the subjects he is modeling.

Bibliography

[Bathe 1995] BATHE. 1995. *Finite Element Procedures*, second edition ed. Prentice Hall.

[Becker and Teschner 2007] BECKER, M., AND TESCHNER, M. 2007. Robust and efficient estimation of elasticity parameters using the linear finite element method. In *SimVis*, 15–28.

[Bianchi et al. 2004] BIANCHI, G., SOLENTHALER, B., SZEKELY, G., AND HARDERS, M. 2004. Simultaneous topology and stiffness identification for mass-spring models based on fem reference deformations. In *In MICCAI 2*.

[Bickel et al. 2007] BICKEL, B., BOTSCH, M., ANGST, R., MATUSIK, W., OTADUY, M., PFISTER, H., AND GROSS, M. 2007. Multi-scale capture of facial geometry and motion. In *ACM Transactions on Graphics (Proceedings of the SIGGRAPH conference)*.

[Bickel et al. 2008] BICKEL, B., LANG, M., BOTSCH, M., OTADUY, M., AND GROSS, M. 2008. Pose-space animation and transfer of facial details. In *SCA '08: Proceedings of the 2008 ACM SIGGRAPH/Eurographics Symposium on Computer Animation*, ACM, New York, NY, USA.

[Bonet and Wood 2008] BONET, J., AND WOOD, R. D. 2008. *Nonlinear Continuum Mechanics for Finite Element Analysis*, second edition ed. Cambridge University Press.

[Bouguet 2006] BOUGUET, J.-Y., 2006. Camera calibration toolbox for matlab, http://www.vision.caltech.edu/bouguetj/calib_doc.

[Carr et al. 2001] CARR, J. C., BEATSON, R. K., CHERRIE, J. B., MITCHELL, T. J., FRIGHT, W. R., MCCALLUM, B. C., AND EVANS, T. R. 2001. Re-

construction and representation of 3d objects with radial basis functions. In *SIGGRAPH '01: Proceedings of the 28th annual conference on Computer graphics and interactive techniques*, ACM, New York, NY, USA, 67–76.

[Engl and Kügler 2003] ENGL, H. W., AND KÜGLER, P. 2003. Nonlinear inverse problems: Theoretical aspects and some industrial applications. *Inverse Problems: Computational Methods and Emerging Applications Tutorials*.

[Gibson and Mirtich 1997] GIBSON, S. F. F., AND MIRTICH, B. 1997. A survey of deformable modeling in computer graphics. Tech. rep., Mitsubishi Electric Research Laboratories.

[Hansen 2007] HANSEN, P. C. 2007. Regularization tools. *Numerical Algorithms 46*, 189–194.

[James and Pai 1999] JAMES, D., AND PAI, D. 1999. Artdefo - accurate real time deformable objects. In *In Proceedings of SIGGRAPH 99*, 65 – 72. AVI Video available at: http://www.cs.cmu.edu/ djames/movies/ArtDefo.avi.

[Micheals and Boult 2000] MICHEALS, R. J., AND BOULT, T. E. 2000. On the robustness of absolute orientation. In *IASTED INTERNATIONAL CONFERENCE ON ROBOTICS AND APPLICATIONS*.

[Müller and Gross 2004] MÜLLER, M., AND GROSS, M. 2004. Interactive virtual materials. In *GI '04: Proceedings of Graphics Interface 2004*, Canadian Human-Computer Communications Society, School of Computer Science, University of Waterloo, Waterloo, Ontario, Canada, 239–246.

[Müller et al. 2002] MÜLLER, M., DORSEY, J., MCMILLAN, L., JAGNOW, R., AND CUTLER, B. 2002. Stable real-time deformations. In *SCA '02: Proceedings of the 2002 ACM SIGGRAPH/Eurographics Symposium on Computer Animation*, ACM Press, 49–54.

[Nealen et al. 2005] NEALEN, A., MUELLER, M., KEISER, R., BOXERMAN, E., AND CARLSON, M. 2005. Physically based deformable models in computer graphics.

[Pai et al. 2001] PAI, D. K., VAN DEN DOEL, K., JAMES, D. L., LANG, J., LLOYD, J. E., RICHMOND, J. L., AND YAU, S. H. 2001. Scanning physical interaction behavior of 3d objects. In *SIGGRAPH '01: Proceedings of the 28th annual conference on Computer graphics and interactive techniques*, ACM, New York, NY, USA, 87–96.

[Terzopoulos et al. 1987] TERZOPOULOS, D., PLATT, J., BARR, A., AND FLEISCHER, K. 1987. Elastically deformable models. *SIGGRAPH Comput. Graph. 21*, 4, 205–214.

[Yu et al. 2001] YU, Z., PRAKASH, E., AND SUNG, E. 2001. Real-time physically-based facial expression animation usingmass-spring system. In *Computer Graphics International 2001*.